RIETVELD based energy-dispersive residual stress evaluation: Analysis of complex stress fields $\sigma_{ij}(z)$

Daniel Apel[a]*, Manuela Klaus[a], Martin Genzel[b] and Christoph Genzel[a]

[a]Helmholtz-Zentrum Berlin für Materialien und Energie, Albert-Einstein-Str. 15, Berlin, 12489, Germany, and [b]Technische Universität Berlin, Germany

Correspondence email: daniel.apel@helmholtz-berlin.de

Keywords: Residual stress analysis; triaxial residual stress state; depth gradients; energy-dispersive diffraction; RIETVELD refinement

Synopsis

Energy-dispersive synchrotron diffraction was applied to analyse the near surface residual stress state in polycrystalline materials. A RIETVELD based formalism is introduced which permits a full triaxial data evaluation and, therefore, even the detection of out-of-plane $\sigma_{33}(z)$ gradients.

Abstract

A method for the evaluation of strongly inhomogeneous residual stress fields in the near surface region of polycrystalline materials is introduced, which exploits the full information content contained in energy-dispersive (ED) diffraction patterns. Based on RIETVELD's data analysis concept the macro-stress induced diffraction line shifts ΔE_{ψ}^{hkl} observed in ED $\sin^2\psi$ measurements are described by modeling the residual stress state $\sigma_{ij}(z)$ in the real space. Therefore, the proposed approach differs substantially from currently used methods for residual stress gradient analysis such as the 'Universal plot' method, which enable access to the LAPLACE stress profiles $\sigma_{ij}(\tau)$. With the example of shot-peened samples made of steel 100Cr6 and Al_2O_3, respectively, it is demonstrated that the simultaneous refinement of all diffraction patterns obtained in a $\sin^2\psi$ measurement with hundreds of diffraction lines provides very stable solutions for the residual stress depth profiles. Furthermore, it is shown that the proposed evaluation concept even allows for considering the residual stress component $\sigma_{33}(z)$ in the thickness direction, which is difficult to detect by conventional $\sin^2\psi$ analysis.

1. Introduction

Residual stress fields in the near surface region of polycrystalline materials and thin films play an important role regarding the material properties (e.g. mechanical properties) under service conditions. During the past decades, various concepts and methods for X-ray residual stress analysis (XSA) based on angle-dispersive (AD) and ED diffraction have been developed and successfully applied, see for example the summaries (Hauk, 1997; Genzel, 2003; Welzel *et al.*, 2005; Birkholz, 2006; Reimers *et al.*, 2008; Mittemeijer & Welzel, 2012). Based on the definition of an average depth $\langle z \rangle$ to which the information extracted from the diffraction lines has to be ascribed the different methods can be classified into two groups: the 'real space' and 'LAPLACE space' methods (Genzel *et al.*, 2012).

The basic idea of the real space methods is to define a gauge volume by slits in the primary and the diffracted beam, respectively. In this way, the origin of the diffracted intensity within the material is assigned to the absorption-weighted centroid of the gauge. By scanning the gauge volume under one or more orientations into or within the sample, strain or stress depth profiles can be obtained (Reimers *et al.*, 1998, Withers & Webster, 2001, Genzel *et al.*, 2011a). Very high resolution with respect to the analysis of real space depth gradients can be achieved by employing micro- and nano-beam techniques provided at 3rd generation synchrotron radiation sources (Di Fonzo *et al.*, 2000; Ice *et al.*, 2011; Stefenelli *et al.*, 2013). Krywka *et al.* (2012) and Keckes *et al.* (2012) used these methods successfully to study lattice strain gradients in thin nanocrystalline hard coatings.

The LAPLACE space methods, on the other hand, make use of BEER-LAMBERT's law which describes the exponential attenuation of X-rays by matter. Performing diffraction experiments in reflection geometry, depth resolution is achieved by stepwise variation of tilt and rotation angles, respectively, leading to a variation of the so called 1/e information depth τ which is defined by the condition that $1 - e^{-1} = 63\%$ of the total diffracted intensity originates from. Due to the exponential beam attenuation all strain and residual stress depth distributions obtained from such experiments are not profiles in the real space but profiles in the LAPLACE space, $\sigma(\tau)$. Consequently, access to the corresponding real space profiles, $\sigma(z)$, requires the application of the inverse LAPLACE transform (ILT). Numerical approaches, however, in most cases fail because the numerical inverse LAPLACE transform (INLT) leads to rather ill-conditioned systems of equations which have to be solved (Craig & Thomson, 1994). Therefore, it is common practice to describe the $\sigma(z)$ depth profiles by polynomial (Ruppersberg *et al.*, 1995) or exponentially damped (Hauk & Krug, 1988) functions which can be easily transformed into the LAPLACE space. The unknown profile parameters are determined by a least squares fit to the experimentally obtained, discrete LAPLACE stress depth distributions. The stability of the solutions achieved by this procedure, however, strongly depends on the quality of the discrete LAPLACE stress data. (Denks *et al.*, 2009) showed that very similar profiles $\sigma(\tau)$ in the LAPLACE

space which were obtained by fitting polynomials of different order to the data may differ significantly with respect to the corresponding real space, $\sigma(z)$.

In this paper a new method for ED residual stress depth gradient analysis based on a recently developed ED RIETVELD program (Apel *et al.*, 2011) is presented. With the example of two mechanically surface treated samples, which differ significantly with respect to their near-surface residual stress distribution, the introduced approach is shown to be applicable to long-range and steep stress gradients as well as to the evaluation of triaxial residual stress fields. The paper is organized as follows: In chapter 2 the fundamental relations of the RIETVELD method for the ED diffraction mode are introduced and a formalism is presented for the refinement of a model which describes the full triaxial near surface residual stress state. Experimental details are given in chapter 3. Here, we also show with the example of a macro stress free standard powder that full ED diffraction pattern refinement needs a correction of the detector dead time induced line shift rather on the channel scale than on the energy scale. The new approach for residual stress depth gradient analysis is tested in chapter 4 on two samples with a different near surface residual stress state to show the general applicability of this new method.

2. Fundamentals of RIETVELD-based energy-dispersive residual stress gradient analysis

2.1. Application of the RIETVELD method to lattice strain evaluation

The fundamental equation of ED diffraction is obtained from BRAGG's equation $n\lambda = 2d^{hkl}\sin\theta$ and PLANCK's energy equation $E = hc/\lambda$ by eliminating the wavelength λ:

$$E^{hkl}(\text{keV}) = \frac{6.199}{\sin\theta}\,\frac{1}{d^{hkl}(\text{Å})}. \qquad (1)$$

It correlates the position E^{hkl} of a diffraction line hkl on the energy scale with the lattice plane distance d^{hkl}. The BRAGG and the diffraction angle, θ and 2θ, respectively, remain fixed during the measurement and can be selected freely.

Recently, a RIETVELD program for the evaluation of the ED diffraction data measured at the materials science beamline EDDI@BESSY II was developed (Apel *et al.*, 2011). The first investigations primarily focused on the determination of microstructural parameters like domain size and microstrain in some standard samples. The program is now enhanced in order to be able to analyse diffraction line shifts for the analysis of residual stress depth gradients. The principle of the RIETVELD method (RIETVELD, 1967, 1969) is to minimize the weighted sum of squared residuals (WSS) of the observed intensities y_i^{obs} of a diffraction pattern and the calculated intensities y_i^{calc} of a model which describes the crystal structure and microstructural properties:

$$WSS = \sum_i w_i \left(y_i^{obs} - y_i^{calc}\right)^2 \quad (2)$$

with $w_i = 1/\sigma_i$ being the weighting factor of the intensity for the i^{th} measuring point in the diffraction pattern. The intensities of the ED diffraction patterns are calculated according to the following ansatz:

$$y_i^{calc} =$$

$$S \sum_{hkl} \left\{ W\left(E^{hkl}\right) A\left(E^{hkl}\right) P\left(E^{hkl}, \theta\right) M^{hkl} \left|F^{hkl}\right|^2 \left(E^{hkl}\right)^{-3} G\left(E_i - E^{hkl}\right) \right\} + y_i^{bkg} \quad (3)$$

(S - scale factor, $W\left(E^{hkl}\right)$ - correction factor for the wiggler spectrum, $A\left(E^{hkl}\right)$ - energy dependent absorption correction, $P\left(E^{hkl}, \theta\right)$ - polarization factor, M^{hkl} - multiplicity of the Bragg reflection *hkl*, F^{hkl} - structure factor, $G\left(E_i - E^{hkl}\right)$ - line profile function, y_i^{bkg} - background intensity).

The line profile G is described by the generalized THOMPSON, COX & HASTINGS (TCH) pseudo-Voigt model (Thompson *et al.*, 1987) which was modified for the ED case of diffraction (Apel *et al.*, 2011):

$$\left(\Gamma_G^{hkl}\right)^2 = P + U \cdot \left(E^{hkl}\right)^2, \quad (4)$$

$$\Gamma_L^{hkl} = X + Y \cdot E^{hkl}, \quad (5)$$

where Γ is the full width at half maximum (FWHM) of the line profile, *P*, *U*, *X*, and *Y* are refinable parameters related to size (*P*, *X*) and strain (*U*, *Y*) broadening, and *G* and *L* denote Gauss and Lorentz profiles, respectively (see (Apel *et al.*, 2011) for details). The calculation of the structure factors F^{hkl} was done using the LE BAIL method (Le Bail *et al.*, 1988).

A macroscopic lattice strain defined by:

$$\varepsilon^{hkl} = \left(d^{hkl} - d_0^{hkl}\right)/d_0^{hkl} = \Delta d^{hkl}/d_0^{hkl} \quad (6)$$

(d_0^{hkl} – strain free lattice parameter) leads to shifts of the diffraction lines, which are given on the energy scale by:

$$\Delta E^{hkl} = E^{hkl} - E_0^{hkl} = -\varepsilon^{hkl} \cdot E_0^{hkl}, \quad (7)$$

where E_0^{hkl} is the line position that corresponds to the diffraction performed on the unstrained lattice with the parameter d_0^{hkl}. With the above equation the line profile function *G* of any reflection *hkl* in equation (3) can be written as:

$$G\left(E_i - E^{hkl}\right) = G\left[E_i - E_0^{hkl}\left(1 - \varepsilon^{hkl}\right)\right]. \quad (8)$$

In general, the lattice strain in polycrystalline samples is anisotropic on the macroscopic as well as on the microscopic (i.e. crystallite) scale. Therefore, the shifts of different lines E^{hkl} in *one and the same* ED diffraction pattern will differ by their magnitude and, in special cases, even by their sign (Greenough, 1949). In the next chapter it is shown how the RIETVELD formalism outlined above can be used to evaluate residual stress depth profiles $\sigma_{ij}(z)$ from ED diffraction lattice strain measurements performed in different orientations with respect to the sample reference system.

2.2. Modeling residual stress-strain relations for depth-resolved RIETVELD data evaluation

Residual stresses in polycrystalline materials are not homogeneous but occur in the form of gradients on different length scales (Macherauch *et al.*, 1973). As a consequence of mechanical surface treatment, for example, the macroscopic and phase specific residual stresses are generated in the topmost material regions that vary with the distance *z* from the surface, resulting in more or less pronounced gradients $\sigma_{ij}(z)$ of individual components of the stress tensor. The correlation between the residual stress fields and the lattice strains ε^{hkl} caused by these residual stress fields is given by HOOKE's law, which reads in a compact form:

$$\varepsilon_{\varphi\psi}^{hkl}(z) = F_{ij}^{hkl}(\varphi,\psi)\cdot\sigma_{ij}(z). \tag{9}$$

In this equation the azimuth angle φ and the inclination angle ψ define the orientation of the diffraction vector $\boldsymbol{g}^{hkl}$ (i.e. of the measuring direction) with respect to the sample reference system, and F_{ij}^{hkl} are the so-called stress factors. For quasi-isotropic polycrystalline materials with random crystallographic texture the F_{ij}^{hkl} can be expressed by the diffraction elastic constants (DEC) S_1^{hkl} and $\frac{1}{2}S_2^{hkl}$. Assuming, for further considerations, a triaxial residual stress state with rotational in-plane symmetry, i.e. $\sigma_{11} = \sigma_{22} = \sigma_{\parallel}$:

$$\boldsymbol{\sigma}(z) = \begin{pmatrix} \sigma_{||}(z) & 0 & 0 \\ 0 & \sigma_{||}(z) & 0 \\ 0 & 0 & \sigma_{33}(z) \end{pmatrix}, \tag{10}$$

equation (9) takes the form:

$$\begin{aligned}\varepsilon_{\psi}^{hkl}(z) &= F_{||}^{hkl}(\psi)\cdot\sigma_{||}(z) + F_{33}^{hkl}(\psi)\cdot\sigma_{33}(z) \\ &= \left(\tfrac{1}{2}S_2^{hkl}\sin^2\psi + 2S_1^{hkl}\right)\cdot\sigma_{||}(z) + \left(\tfrac{1}{2}S_2^{hkl}\cos^2\psi + S_1^{hkl}\right)\cdot\sigma_{33}(z)\end{aligned} \tag{11}$$

Due to the exponential attenuation of the X-rays by matter given by BEER-LAMBERT's law the lattice strain profiles $\varepsilon_{\psi}^{hkl}(z)$ are not directly accessible from diffraction experiments. Instead, the measured signal has to be assigned to an average information depth τ which is defined by the condition that 1 –

e^{-1} = 63% of the total diffracted intensity originates from a surface layer of thickness τ. For the symmetrical Ψ–mode of X-ray stress analysis τ is given by:

$$\tau\left(E^{hkl},\theta,\psi\right)=\frac{\sin\theta}{2\mu\left(E^{hkl}\right)}\cos\psi\ . \tag{12}$$

Since the effective linear absorption coefficient μ depends on the photon energy, the lattice strain obtained from *different* reflections E^{hkl} in the ED diffraction pattern has to be assigned to *different* information depths $\tau\left(E^{hkl},\theta,\psi\right)$. The correlation between the experimentally accessible lattice strain and residual stress depth profiles $\varepsilon_{\psi}^{hkl}(\tau)$ and $\sigma_{ij}(\tau)$, respectively, and the actual (real space) profiles $\varepsilon_{\psi}^{hkl}(z)$ and $\sigma_{ij}(z)$ is given by the transform:

$$\varepsilon_{\psi}^{hkl}(\tau)=\int_0^{\infty}\varepsilon_{\psi}^{hkl}(z)\,e^{-\frac{z}{\tau}}dz\Big/\int_0^{\infty}e^{-\frac{z}{\tau}}dz \tag{13}$$

$$\sigma_{ij}(\tau)=\int_0^{\infty}\sigma_{ij}(z)\,e^{-\frac{z}{\tau}}dz\Big/\int_0^{\infty}e^{-\frac{z}{\tau}}dz \tag{14}$$

For bulk samples of thickness $D \gg \tau$ the above integral equation has the form of a LAPLACE transform. Therefore, the strain and stress depth profiles which are *directly* obtained from diffraction experiments are called 'LAPLACE-profiles'.

Taking into account the depth dependency of the strains and stresses, and making use of equations (13) and (14) the line profile function (8) becomes:

$$\begin{aligned}G\left(E_i-E_{\psi}^{hkl}\right)&=G\left\{E_i-E_0^{hkl}\left[1-\varepsilon_{\psi}^{hkl}(\tau)\right]\right\}\\&=G\left\{E_i-E_0^{hkl}\left[1-F_{ij}^{hkl}(\psi)\cdot\int\sigma_{ij}(z)\,e^{-\frac{z}{\tau}}dz\Big/\int e^{-\frac{z}{\tau}}dz\right]\right\}.\end{aligned} \tag{15}$$

This equation correlates the peak position E_{ψ}^{hkl} of any diffraction line *hkl* in an ED diffraction pattern obtained for a measuring direction ψ directly with the actual depth profiles of the residual stress tensor components σ_{ij} in the real or *z*-space.

The RIETVELD strategy for residual stress gradient analysis from ED diffraction experiments is illustrated in Fig. 1. The main feature of this approach is that a*ll* diffraction patterns and, therefore, *all* diffraction lines measured for $\sin^2\psi$-based XSA are refined *simultaneously* by a non-linear least-squares method using the 'trust-region-reflective' algorithm to determine the parameters a_0, a_1 … a_n. According to equation (12) each diffraction line E^{hkl} can be ascribed to a different information depth τ. Considering, for example, the case that diffraction patterns have been measured under 30 different ψ angles and that 8 diffraction lines E^{hkl} per diffraction pattern are available for analysis this would mean that the parameters a_0, a_1 and a_2 are refined based on the information of 240 diffraction lines or

about $5{\cdot}10^5$ data points (cf. Fig. 1). The refined parameters then can be used directly to calculate the residual stress depth distribution in real space, $\sigma_{ij}(z)$. Typical functions used to describe $\sigma_{||}(z)$ and their LAPLACE transform are summarized in Tab. 1.

[Figure 1]

The 'goodness' of the refined model is assessed by (a) the residuals obtained for the fitted diffraction patterns and (b) the closeness of agreement between the $d_{\varphi\psi}^{hkl}$ vs. $\sin^2\psi$ plots evaluated from the experiment and the $d_{\varphi\psi}^{hkl}(\sin^2\psi)$-curves recalculated from the refined model according to:

$$d_{\psi}^{hkl} = \left(\frac{1}{2}S_2^{hkl}\sin^2\psi + 2S_1^{hkl}\right)\sigma_{||}\left(\tau^{hkl}\right)d_0^{hkl} + d_0^{hkl}, \qquad (16)$$

if a biaxial residual stress state of rotational symmetry is assumed for the near surface material region. During the RIETVELD refinement the lattice parameter is held constant at a previously determined value. The so-called 'strain-free lattice parameter' is determined by interpolation of the respective d_{ψ}^{hkl}–$\sin^2\psi$–distribution in the strain-free direction $\psi^{*,hkl}$, which is given by:

$$\psi^{*,hkl} = \sin^{-1}\sqrt{-2S_1^{hkl}/\left(\tfrac{1}{2}S_2^{hkl}\right)}\,, \qquad (17)$$

or, if available, from a standard (unstrained) reference sample of the material under investigation. The d_{ψ}^{hkl}–$\sin^2\psi$–distribution is determined through least-squares refinement of $\varepsilon_{\psi}^{hkl}(\tau)$ (equation (13)), with $\varepsilon_{\psi}^{hkl}(\tau)$ being treated as a single refinable parameter for each diffraction line E^{hkl}. That means that no model to describe the residual stress depth distribution $\sigma_{||}(z)$ is assumed and that the shift of each diffraction line is determined separately.

In general, the traditional XSA methods assume a biaxial stress state in the volume sampled by the X-ray beam, whereas stress components in the direction of the surface normal are neglected. However, it has been shown in several studies (Dölle & Cohen, 1980; Cohen *et al.*, 1980, Ruppersberg, 1997) that this assumption is not justified in either case. It is known that the presence of shear stress components σ_{13} and σ_{23} results in a splitting of the d_{ψ}^{hkl}–$\sin^2\psi$–distribution, i.e. the d_{ψ}^{hkl}–$\sin^2\psi$–distributions have opposite curvature for positive and negative ψ. By (Noyan, 1983) it was shown that a normal stress component σ_{33} perpendicular to the surface in absence of shear stresses leads to a curvature of the d_{ψ}^{hkl}–$\sin^2\psi$–distribution and no ψ-splitting occurs. It was shown further that neglecting even small curvatures caused by σ_{33} could lead to appreciable errors in the calculated surface stress.

The stress component σ_{33} in the direction of the surface normal has to obey the boundary conditions $\sigma_{33}(z=\tau=0)=0$ and $\partial\sigma_{33}(z=0)/\partial z = 0$ .We do not consider here the shear components

σ_{13} and σ_{23}, because they can be extracted (separated) easily from the fundamental equation of XSA by adding (subtracting) the strain or lattice spacing profiles measured in the positive and negative ψ–direction, respectively. The following functions, which fulfill the requirements imposed by the boundary conditions, were used to model the σ_{33} component in real space and LAPLACE space, respectively:

$$\sigma_{33}(z) = az^3 e^{-bz}, \quad (18)$$

$$\sigma_{33}(\tau) = 6a\tau^3/(b\tau + 1)^4, \quad (19)$$

where *a* and *b* are refinable parameters. According to the characteristics of this function, it is assumed that the σ_{33} component reaches a maximum below the materials surface and then approaches zero going further away from the surface into the material. Thus, the amplitude of the curve is specified by the parameter *a* and the damping of the curve is specified by parameter *b*. Simultaneously refining all parameters of the functions used to describe $\sigma_{||}(z)$ and $\sigma_{33}(z)$, respectively, permits a full triaxial residual stress gradient analysis.

3. Experimental

3.1. Energy-dispersive synchrotron diffraction

The ED diffraction experiments were carried out using the white high energy synchrotron radiation provided at the materials science beamline EDDI@BESSY II in Berlin, details on the experimental setup may be found in (Genzel *et al.*, 2007). A N_2 (liq.)-cooled energy-dispersive solid state low energy germanium detector (Canberra model GL0110) was used for data acquisition. The applicability for ED experiments and properties of this detector were studied in detail by (Denks & Genzel, 2007, Denks & Genzel, 2008; Genzel *et al.*, 2011). In (Denks & Genzel, 2008) it was shown that the variation of the detector dead time DT - during a $\sin^2\psi$ measurement leads to systematic diffraction line shifts giving rise to ‘ghost-stresses’ which would falsify the XSA results. The DT denotes the timespan immediately after the detection of an event in which the detector is not ready to detect another event, i.e. the minimum time needed to separate two successive events. In the case of an energy-dispersive detector the event to be detected is measuring the incoming photons. Usually, the DT is given in percent [%], calculated according to the formula

$$DT\ [\%] = (1 - \text{life time}/\text{measurement time}) \times 100\% \quad (20)$$

where the life time [s] denotes the actual time where photons are being measured and the measurement time [s] denotes the total time used to accumulate the spectrum. During the experiments described in this paper it was noticed that the currently applied dead time correction needs to be

improved. Therefore a modified approach to correct for the variation of the detector dead time during a $\sin^2\psi$ measurement is introduced in this paper (section 3.2).

The ED measurements focused on $\sin^2\psi$-based residual stress investigations performed in the Ψ-mode of XSA. ED diffraction data were recorded within an energy range of approximately 15 - 80 keV. For the measurements on the 100Cr6 steel sample and the Al_2O_3 sample diffraction angles $2\theta = 16°$ and $2\theta = 11°$, respectively, were chosen. The measurement time for the diffraction patterns was 30 s for the 100Cr6 sample and 300 s for the Al_2O_3 sample. The primary beam cross section was set to 0.5 x 0.5 mm² and on the secondary side the apertures of the two-slit system were adjusted to 0.03 x 5 mm² (equatorial x axial) in order to prevent geometrically induced line-broadening and to restrict line-shifts to $\Delta 2\theta < 0.01°$. For the determination of the instrumental broadening the reference material LaB_6 SRM660b (NIST) was measured using the identical diffraction setup that was used for the $\sin^2\psi$ measurements on the samples discussed in this paper.

3.2. Enhanced dead time correction

The evaluation of the actual (i.e. lattice strain and stress induced) energy diffraction line positions, which are corrected for all instrumental effects, in particular for those being related to the detector electronics is of utmost importance for the ED residual stress analysis. The analysis of residual stresses requires the determination of lattice strains in the range of $\varepsilon = [10^{-3} \ldots 10^{-5}]$. Therefore, the determination of energy positions for the photon energies available at the EDDI beamline (up to 100 keV) must be accurate within ≤ 10 eV.

To investigate the influence of the dead time on the measured energy positions, $\sin^2\psi$ measurements on a standard gold powder (a_0^{Au} = 0.4078 nm) were conducted. In Fig. 2 the shift $\Delta E = \left(E_\psi^{hkl} - E_0^{hkl}\right)/E_0^{hkl}$ with regard to the theoretical energy positions E_0^{hkl} of the Au diffraction lines is shown as a function of dead time. For the determination of ΔE the uncorrected raw data as received from the ED detector were used. It can be seen that there is a significant deviation from the theoretical energy positions not only as a function of dead time but also depending on the reflections *hkl*, i.e. on the absolute energy positions. The currently applied dead time correction only corrects successfully for the dead time induced shift of the *individual* energy positions whereas the obvious *hkl* dependency was first noticed when the RIETVELD method was applied to the ED diffraction data. The latter would indicate different lattice parameter values a^{hkl} for the individual diffraction lines E^{hkl} of Au. The deviations between the diffraction lines are more or less independent of the dead time. This finding indicates that the assignment of the channel number *ch* of the multichannel analyzer (MCA) to the actual photon energy *E* is incorrect.

[Figure 2]

Therefore, to assign the channel number *ch* to the actual photon energy *E* the following equation is used:

$$E(ch) = a + b \cdot ch + c \cdot ch^2, \quad (21)$$

where the parameters *a*, *b* and *c* are determined using different energy standards, e.g. the emission lines of radionuclides like ^{241}Am or ^{133}Ba as well as the fluorescence lines of different elements where the theoretical energy positions are known with sufficient accuracy. It will be shown in the following, that the erroneous assignment of the channel numbers *ch* to the actual photon energies *E* is due to the procedure used so far for detector calibration. Until now the channel (energy) positions of the emission and fluorescence lines of the different standards were determined for *different* dead times. Instead of applying the dead time correction to the shift ΔE of the diffraction lines on the energy scale (Genzel *et al.*, 2011) it is more convenient to apply it to the shift Δch observed on the channel scale.

The approach used to determine the proper dead time correction reads as follows: The radionuclides were taped together directly in front of the detector window and a spectrum was recorded. The resulting dead time and the channel numbers determined from this spectrum are used as reference values. By varying the distance of the standard materials to the detector window and carrying out $\sin^2\psi$ measurements different dead times between 0.08 % and 33 % were realized. Then, for each dead time the peak maximum channel numbers of the emission and fluorescence lines were determined. In the next step, these values were corrected using the respective channel positions determined for the reference dead time. The resulting dead time induced shift Δch of the channel number shows no systematic deviation in one specific direction. Therefore, the shift Δch can be considered independent of energy. To describe to describe the line shift vs. dead time distribution the following exponential function was fitted to the experimental data:

$$y = y_0 + A_1 \exp(-x/t_1), \quad (22)$$

resulting in the values y_0 = -2.91412, A_1 = 6.34603 and t_1 = 7.44829 [s]. These parameters were used for the dead time correction of all experiments presented in this paper. By using this correction function a line shift Δch can be calculated for the dead time x of the respective measurement under investigation. This shift Δch is then added to the channel numbers of the emission and fluorescence lines determined for the reference dead time. The corrected channel numbers are then used to determine the parameters *a*, *b* and *c* of equation (21) that is used to assign the channel numbers to the actual photon energies. Whereas the dead time correction applied so far used only one set of parameters *a*, *b* and *c* for *all* dead times the new dead time correction yields a set of parameters for *each* dead time. In Fig. 3 the dead time dependency of the parameters of equation (21) is shown. It

can be seen that only the parameter *a* strongly depends on the dead time whereas the parameters *b* and *c* are independent of the dead time.

[Figure 3]

Applying the enhanced dead time correction to the calibration measurement shown in Fig. 2, the deviation ΔE from the theoretical energy positions E_0^{hkl} was reduced significantly not only with regard to the dead time but also with regard to the absolute energy position, as shown in Fig. 4. This is particularly important in view of the application of the RIETVELD method to the analysis of ED diffraction spectra, since the energy positions of all diffraction lines are calculated using one and the same lattice parameter a_0. The deviation ΔE of the different diffraction lines from the theoretical line positions inside a single spectrum, which was obtained as a consequence of the dead time correction used up to now (cf. Fig. 2), would make a reliable refinement of the materials structure almost impossible.

[Figure 4]

3.3. Samples

The main goal of this paper is to introduce the enhancement of the RIETVELD program developed by (Apel *et al.*, 2011) with regard to the analysis of residual stress depth gradients. Investigations were performed on a steel 100Cr6 and an α-Al_2O_3 ceramic, which differ significantly with respect to the residual stress state that was introduced by mechanical surface treatment. Both materials were ground and subsequently shot-peened to generate residual stress fields within the near surface region which are inhomogeneous with respect to the depth *z*. Details of the sample treatment are summarized in Table 2.

[Table 2]

Preliminary X-ray diffraction and EBSD investigations revealed that the samples are free of preferred crystallographic texture. The residual stress state of both samples was extensively studied using both AD and ED diffraction analysis methods (Genzel *et al.*, 2011). The studies showed that the in-plane residual stress state of both samples is of rotational symmetry but significant differences were found with respect to the magnitude, extension and steepness of the gradients, respectively. Thus, the samples are well suited to test the applicability of the RIETVELD model for the analysis of residual stress depth gradients for a rather long-range and an extremely steep residual stress gradient. The diffraction elastic constants S_1^{hkl} and $\frac{1}{2}S_2^{hkl}$ needed for residual stress evaluation were calculated

using the single crystal elastic constants (Landolt-Börnstein, 1979) on the basis of the Eshelby-Kröner model (Eshelby, 1957; Kröner, 1958).

4. Results and discussion

4.1. Residual stress distribution with moderate gradient: Shot-peened steel 100Cr6

Preliminary X-ray diffraction investigations including the stress-scanning method (Denks, 2008) and the layer removal method (Manns, 2010) (on a sample from the same batch), that allow for determination of the real space residual stress depth profile $\sigma_{||}(z)$, revealed the introduction of compressive residual stresses in the near surface region of the sample. The $\sigma_{||}(z)$ profiles obtained by both methods are shown in Fig. 5. The residual stress depth profile $\sigma_{||}(z)$ is characterized by a pronounced maximum of about -1250 MPa compressive stress at about 30 µm below the surface followed by a decrease of the compressive stresses with increasing depth. The $\sigma_{||}(z)$ profiles obtained by the real space methods provide the basis for the assessment of the residual stress depth profile obtained by means of residual stress depth gradient analysis on the basis of the RIETVELD method introduced in this paper.

[Figure 5]

The results of the simultaneously RIETVELD refined ED diffraction patterns according to the concept outlined in Section 2.2 are shown in Fig. 6 for selected ψ angles. For $\psi \leq 82°$ six diffraction lines and for $82° > \psi \leq 85°$ two diffraction lines (110 and 211) were used for the analysis. That results in a total of 156 diffraction lines or about 500.000 data points that were used simultaneously for the evaluation of the residual stress depth gradient. To model $\sigma_{||}(z)$ an exponentially damped polynomial function of first order, $\sigma_{||}(z) = (a_0 + a_1 z)e^{-a_2 z}$, was used. The strain-free lattice parameter a^{100} = 0.28679 nm was used for the refinement, predetermined using the strain-free direction ψ^* (see equation (17)). As can be seen from the residuals of the refined ED diffraction patterns, the energy positions of the different diffraction lines are all well-matched, even under grazing diffraction conditions (ψ = 82° – 86°).

[Figure 6]

From the RIETVELD refinement the residual stress depth profiles in both, the LAPLACE- and real space are available. Fig. 7 compiles the residual stress depth profiles evaluated by means of the RIETVELD method and the direct real space approach, i.e. the stress scanning method. A good match between the real space profile $\sigma_{||}(z)$ obtained by the stress scanning method and the RIETVELD method is

observed. This applies at least for the 'main τ-range' marked in the diagram, which indicates the range where the major part of the experimentally accessible diffraction information originates from. For depths larger than about 70 µm the RIETVELD refinement yields results which differ considerably from the direct real space approach. The deviations between the real space profiles obtained from the stress scanning method and the RIETVELD method for large τ values can be explained considering the accessible information depth (τ, z) of each method. The stress scanning method is based on through surface strain scanning in the ED diffraction mode using a small gauge volume of about 10 µm height. It yields a discrete profile of the residual stress component even in large depths z without changing the orientation between the gauge volume and the sample. The accessible information depth achieved by the RIETVELD method, on the other hand, is limited by the exponential attenuation of the X-rays by matter. In this case the maximum information depth τ refers to the 321 diffraction line at $\psi = 0°$. Furthermore, the data density of the LAPLACE stress data being used for the evaluation is much higher for smaller information depths τ than in the deeper material zones, see Fig. 7. Consequently, deeper material zones are 'not well represented' in the evaluation leading to the observed differences in larger depths z.

[Figure 7]

The correctness of the refined model can be assessed by comparing the discrete d_ψ^{exp} vs. $\sin^2\psi$ distributions, which are obtained from whole pattern fitting without assuming a residual stress model, with the $d_\psi^{hkl}(\tau)$ curves that are to be calculated from the refined model $\sigma_{||}(z)$. The corresponding plots are shown in Fig. 8. It can be seen that the calculated $d_\psi^{hkl}(\tau)$ curves are in good agreement with the experimental d_ψ^{exp} vs. $\sin^2\psi$ curves, throughout the whole ψ range. Even the curvature at higher ψ angles, resulting from the residual stress gradient, is well described by the refined model. Additionally, the observed deviation between the refined model function and the experimental data is expressed in terms of energy, ΔE, in order to have another criterion to assess the quality of the model. It can be seen that the deviations are not larger than 10 eV – 15 eV, except for the 321 diffraction line ($\Delta E \leq 20$ eV), which is the one with the lowest intensity at all ψ angles. Therefore, the deviations are reasonable within the total experimental error and the refined model for $\sigma_{||}(z)$ can be regarded reliable.

[Figure 8]

The RIETVELD refinement was repeated using exponentially damped polynomial functions of higher order (P2 and P3 from Tab. 1) to model $\sigma_{||}(z)$ and the results are shown in Fig. 9. It is seen that the evaluation yielded almost identical $\sigma(z)^{Rietveld}$-profiles, showing the stability of the residual stress analysis using the RIETVELD method. When applying methods which calculate the real space profile $\sigma(z)$ by fitting their LAPLACE transform to the experimentally determined, discrete LAPLACE stress

data $\sigma(\tau)$, the stability of the back transform is often problematic (Denks *et al.*, 2009). In many cases, strongly scattering LAPLACE space data prevent from finding stable and reliable solutions. By using all the available experimental data simultaneously for the least-squares fit procedure of the RIETVELD method the scattering of the experimental data can be compensated and the evaluation procedure is less influenced by the scattering than other LAPLACE space methods, as with e.g. the universal-plot method (Ruppersberg *et al.*, 1989), where the amount of data that can be used for the evaluation is further restricted due to numerical problems that arise for residual stress data obtained for small ψ angles as well as ψ positions close to the strain-free direction ψ^*.

[Figure 9]

For the determination of the out-of-plane component $\sigma_{33}(z)$ the two parameters *a* and *b* from equation (18) were refined. As described in section 2.2 the refinement was done the following way: both parameters of equation (18) were refined together with the parameters of the model function used to describe $\sigma_{||}(z)$. The in-plane component $\sigma_{||}(z)$ was again described using the function P1 from Tab. 1. The resulting parameter values from the RIETVELD refinement of the respective stress tensor components are summarized in Tab. 3. The parameters of $\sigma_{||}(z)$ refined together with $\sigma_{33}(z)$ show only small deviations from the parameters obtained from the refinement without considering the out-of-plane component $\sigma_{33}(z)$. Furthermore, it should be noted that the parameters *a* and *b* take on very small values. Considering the fit uncertainties being almost of the same magnitude as the refined parameters one can conclude that no significant $\sigma_{33}(z)$ component is present in the mechanically treated surface zone of this sample. This finding agrees with theoretical considerations based on continuum mechanics. Since the amount of cementite in this sample, which would act as second phase and, therefore, give rise to the occurrence of "pseudo-macro" (PM) stresses $\sigma_{33}^{\alpha}(z)$ (Noyan & Cohen, 1987) can be neglected, one can assume a homogeneous macrostress tensor. This means that the boundary conditions $\sigma_{33}(z = \tau = 0) = 0$ and $\partial\sigma_{33}(z = 0)/\partial z = 0$ being valid for the (almost) single phase ferritic steel must result in $\sigma_{33} \equiv 0$ at any depth below the surface of this single-phase material.

[Table 3]

4.2. Residual stress distribution with steep gradient: Shot-peened Al_2O_3

The Al_2O_3 ceramic sample has been the subject of many investigations regarding the application of established and newly developed methods for ED residual stress depth gradient analysis (Genzel *et al.*, 2011; Meixner *et al.*, 2013). Therefore, the near surface residual stress state of the sample is well known and it is particularly suited to test the applicability of the RIETVELD method to an “extreme”

case of a residual stress gradient. The residual stress state is characterized by a very steep gradient showing high compressive stresses at the surface up to about -8 GPa which are balanced by tensile stresses within the first microns below the surface. This kind of residual stress state (very high compressive stresses balanced by tensile stresses within the first few microns below the sample surface) was also found in ceramic multilayer systems (Klaus et al., 2008). The origin of the steep gradient of residual stress is not yet fully understood but it would be beyond the scope of the present paper to elucidate this phenomenon. Here, further studies are necessary, which have to be accompanied by other analytical techniques.

The very short range of the gradient only affects the diffraction lines E^{hkl} corresponding to a small information depth τ. In the present case, the most affected reflections are the 012, 104 and 110 diffraction lines. Consequently, only few data points in the "zone of interest" below the surface are available for the analysis of the residual stress depth gradient. Therefore, only the aforementioned three diffraction lines are used for the evaluation. Since the stress gradient is limited to small information depths, only diffraction patterns recorded at ψ angles $\psi > 70°$ are used for the RIETVELD refinement. Results of the RIETVELD refinement for selected ψ angles are shown in Fig. 10. The agreement between the calculated and the observed profiles is good, even for the highest inclination angle $\psi = 89°$. The stress free lattice parameters used for the RIETVELD refinement were a^{100} = 0.475609 nm and c^{001} = 1.29902 nm, previously determined from the strain-free direction ψ^*. An exponentially damped polynomial of first order (P1 in Tab. 1) was used to describe the real space residual stress depth profile $\sigma_{||}(z)$.

[Figure 10]

The LAPLACE and real space residual stress depth profiles calculated using the refined parameters a_0, a_1 and a_2 from the model function $\sigma_{||}(z)$ are shown in Fig. 11. The refined real space profile $\sigma_{||}(z)$ reveals a very steep gradient of compressive residual stress in the sample. At the surface $z = 0$ a compressive stress of about -8.5 GPa is observed which is balanced by tensile stresses within a depth of 2.5 µm below the surface. At a depth z of about 10 µm the in-plane residual stress approaches zero. These findings are in very good agreement with the results from previous investigations (see e.g. (Meixner *et al.*, 2013)).

[Figure 11]

To assess the quality of the fit the d_ψ^{exp} vs. $\sin^2\psi$ distributions obtained by RIETVELD refinement of the ED diffraction patterns without assuming a residual stress state are compared again to the $d_\psi^{hkl}(\tau)$ curves calculated from the refined model $\sigma_{||}(z)$. The corresponding plots are shown in Fig. 12. It can

be seen that the calculated $d_\psi^{hkl}(\tau)$ curves are in very good agreement with the experimental d_ψ^{exp} vs. $\sin^2\psi$ plots throughout the whole ψ range, although the diffraction patterns for $\psi < 70°$ have not been used for the evaluation. This confirms the assumption about the small depth range of the residual stress gradient, which led to the exclusion of the diffraction patterns recorded for $\psi < 70°$. The strong curvature at higher ψ angles ($\psi > 82°$), which results from the very steep residual stress gradient, is well described by the refined model $\sigma_{||}(z)$ for all three diffraction lines. The observed deviations ΔE between the refined model function and the experimental data is less than about ±5 eV up to $\sin^2\psi \approx 0.99$ and about ±10-20 eV for higher ψ angles $\psi > 85°$. Therefore, the refined model for $\sigma_{||}(z)$ can be regarded as accurate.

[Figure 12]

To check the stability of the results of the RIETVELD method the refinement was repeated using exponentially damped polynomials of higher order (P2 – P4, see Tab. 1). The resulting LAPLACE and real space residual stress depth profiles are shown in the inset of Fig. 11. The different functions yield almost identical results for the residual stress depth profile indicating that the order of the polynomial function used to model $\sigma_{||}(z)$ has a negligible influence on the results obtained by the RIETVELD refinement. This highlights the robustness of the analysis method applied here, as already observed for the 100Cr6 sample in the previous chapter.

4.3. Simulation and analysis of a triaxial residual stress state

In section 4.1 the refinement of the out-of-plane stress tensor component $\sigma_{33}(z)$ showed that this component is negligible for the ferritic steel sample. In order to investigate how the RIETVELD based approach for residual stress gradient analysis works in presence of a triaxial stress state, a simulation for strongly non-uniform triaxial residual stress distributions $\sigma_{ii}(z)$ $(i = 1,2,3)$ was performed. The simulations were carried out for a polycrystalline steel sample (strain-free lattice parameter $a_0 = 0.28679$ Å) with random texture. A depth gradient of the chemical composition which would give rise to a gradient $d_0(z)$ of the strain-free lattice parameter was excluded from the considerations, because it would have the same effect as a hydrostatic residual stress component. As a consequence, additional information on the depth profile of the chemical composition of the material is required in order to separate compositional and residual stress gradients.

The following stress tensor $\sigma(z)$ in the z-space, which was also used in (Genzel *et al.*, 2004) for simulation experiments, was assumed for the simulations:

$^2\vec{\sigma}(z)(\mathrm{MPa})$

$$= \begin{pmatrix} (-1000 + 50z^2)e^{-0.4z} & 0 & 0 \\ 0 & -500 & 0 \\ 0 & 0 & 20z^3 e^{-0.4z} \end{pmatrix}. \quad (23)$$

For the components σ_{11} and σ_{33} steep residual stress gradients was assumed, where the latter has to obey the boundary conditions $\sigma_{33}(z = \tau = 0) = 0$ and $\partial\sigma_{33}(z = 0)/\partial z = 0$. The component σ_{22} was assumed to be constant in depth. The respective depth profiles are shown in Fig. 13. The corresponding stresses in the $\tau -$ or Laplace space, $\sigma_{ii}(\tau)$, were calculated by means of Eq. 14.

[Figure 13]

The diffraction patterns were calculated according to Eq. 3 using the atomic scattering factors from (Brown *et al.*, 2006) considering the 110, 200, 211, 220, 310, 222 and 321 diffraction lines. The simulations were carried out for the ED diffraction mode and the symmetrical Ψ mode of the XSA for 2θ = 16° in the azimuths φ = 0° and 90° with 32 steps in ψ, with $0° < \psi \leq 89°$, respectively. This means a total of 64 diffraction patterns were taken onto account for the simulations. In order to get a realistic idea of the situation, some noise was superimposed to the intensity profiles and additionally, the scale factors were chosen in a way that they decrease with increasing ψ angle, resulting in more or less realistic diffraction patterns (see Fig. 15).

[Figure 14]

For the RIETVELD refinement all 64 diffraction patterns were refined simultaneously using an exponentially damped polynomial function of 4th order

$$\sigma_{ii}(z) = \left[a_0^{(ii)} + a_1^{(ii)} z + a_2^{(ii)} z^2 + + a_3^{(ii)} z^3 + a_4^{(ii)} z^4 \right] e^{-a_5^{(ii)} z} \quad (24)$$

to describe each of the three components in the stress tensor ${}^2\vec{\sigma}(z)$. This means that the refinement was done with "flexible" models for the residual stress depth distribution, i.e. without assuming profiles that are similar to the defaults. First, all six parameters of the polynomial functions of the individual stress tensor components (for the σ_{33} component the parameter $a_0^{(33)}$ was set to zero, due to the boundary conditions) were each refined separately. In the next step the parameters of the polynomial functions of all stress tensor components were refined together. After each refinement circle the resulting residual stress depth profiles were assessed graphically. An overshooting of the residual stress depth profiles was observed during the initial stages of the refinement. Therefore, the number of parameters of the polynomial functions was reduced stepwise and separately for each stress tensor component. After each refinement circle the residual stress depth profiles were assessed again graphically till no more overshooting was observed. The refined diffraction patterns are shown in Fig.

14. The final refinement result for the residual stress depth profiles of the individual stress tensor components and the results of some intermediate steps are shown in Fig. 15.

[Figure 15]

The stress tensor $\sigma(z)$ obtained from the RIETVELD refinement is:

$$^{2}\vec{\sigma}(z)(\mathrm{MPa}) = \begin{pmatrix} (-1051.3 + 217.5z)e^{-0.26z} & 0 & 0 \\ 0 & -522.4 & 0 \\ 0 & 0 & 35.4z^{2}e^{-0.23z} \end{pmatrix}. \quad (25)$$

Although the stress tensor obtained from the RIETVELD refinement is slightly different compared to the default one, a good agreement of the residual stress depth profiles between the two of them is found, see Fig. 16. The differences result from the fact that the refinement was carried out without any specific assumptions with respect to the profile shape of the individual stress components. The results shown in Fig. 16 imply that the approach for the depth dependent analysis of stress tensor components introduced in this paper is a promising alternative to the methods used in (Genzel *et al.*, 2004) for the analysis of multiaxial residual stress fields. Moreover, to the author's knowledge, this is the first time that it is described in literature how to use the RIETVELD method and conventional $\sin^2\psi$ data for this kind of analysis.

[Figure 16]

For the simulations the same refinement strategy was chosen as it would have been used for the analysis of a real sample with an unknown residual stress tensor. At this point, besides the graphical assessment of the quality of the refined model, the assessment based on the comparison of the experimentally obtained d_{ψ}^{exp} vs. $\sin^2\psi$ distributions and the $d_{\psi}^{hkl}(\tau)$ curves recalculated from the refined model $\sigma(z)$ displays its usefulness. In Fig. 17 the simulated d_{ψ}^{exp} vs. $\sin^2\psi$ distribution and the recalculated $d_{\psi}^{hkl}(\tau)$ curves of the 110 diffraction line are shown for some intermediate steps and the final step of the refinement. It can be seen that after the first step of the refinement the deviations between both curves are fairly large indicating that the refined model is not good enough to describe the actual residual stress state. With further steps of the refinement the agreement between both curves improves leading to a very good agreement for the final step of the refinement. It follows that by applying these two "quality controls", a proper refinement strategy to obtain the actual residual stress tensor can be found.

5. Concluding remarks

A new approach for the analysis of residual stress depth gradients from ED diffraction patterns using the recently developed RIETVELD program (Apel *et al.*, 2011) is introduced. The RIETVELD method is used to analyze complete diffraction patterns, which makes this method particularly suitable to be used for the evaluation of ED diffraction data. Furthermore, an enhanced detector dead time correction is introduced to correct the ED diffraction data to avoid electronically introduced E^{hkl} dependent diffraction line shifts.

The approach introduced here makes use of the fact that each diffraction line E^{hkl} in the ED diffraction pattern is subject to a different attenuation and therefore, has to be assigned to a different information depth. During the RIETVELD refinement, parameters related to models describing the depth dependence of the stress tensor components $\sigma_{ij}(z)$ in the real space are adjusted together with other refinable parameters to fit multiple diffraction patterns (measured under different specimen orientations) simultaneously. The approach was tested on samples with well-known residual stress states which differ in range and magnitude, respectively. By comparing the results from the RIETVELD refinement with results from real space (100Cr6 sample) and conventional LAPLACE space methods (α-Al_2O_3 sample) it could be shown that very stable and reliable results can be obtained applying the RIETVELD method for the analysis of residual stress depth gradients. Furthermore, the results from the previous sections show that since the new approach based on the RIETVELD method evaluates a much larger quantity of data (some 10^5 intensities) it is less prone to scattering of the experimental data compared to conventional LAPLACE space methods which calculate the real space profile $\sigma(z)$ by fitting their LAPLACE transform to the discrete LAPLACE stress data. Therefore, the RIETVELD method yields more stable and robust results.

With a simulated example, it has been shown that the new approach for residual stress gradient analysis introduced here can be used in principle for a full analysis of a triaxial residual stress state. However, the more stress tensor components are considered, the more parameters have to be adjusted during the refinement, which is why the refinement strategy needs to be chosen carefully. Nevertheless, by applying the proposed graphical as well as computational quality controls a proper refinement strategy can be found even for complex residual stress states.

As residual stress gradients are often entailed with changes in the microstructure, current studies deal with the development of models to describe the depth dependence of microstructural features, like microstrain and domain size. Those models can be easily implemented in the RIETVELD program to increase its versatility.

Acknowledgements The authors would like to thank Prof. Scholtes and his group for the long-standing fruitful cooperation in the field of X-ray residual stress gradient analysis. Special thanks go to Dr. Th. Manns (now WALTER AG Tübingen) for providing the results on the layer removal investigations performed on the ferritic steel sample shown in Fig. 5.

References

Apel, D., Klaus, M., Genzel, Ch., Balzar, D. (2011). *Z. Kristllogr*. **226**, 934 – 943.

Birkholz, M. (2006) *Thin Film Analysis by X-Ray Scattering*. Wiley-VCH, Weihnheim.

Brown, P. J., Fox, A. G., Maslen, E. N., O'Keefe, M. A., Willis, B. T. M. (2006). International Tables for Crystallography **Vol. C**, Chapter 6.1, 554 – 595.

Cohen, J. B., Dölle, H., James, M. R. (1980). *National Bureau of Standards Special Pubplication* **567**, 453 – 477.

Craig, I. J. D. & Thompson, A. M. (1994). *Computers in Physics* **8**, 648 – 654.Denks, I. A. & Genzel, Ch. (2007). *Nucl. Instrum. Methods in Phys. Research* **B262**, 87 – 94.

Denks, I. A. & Genzel, Ch. (2008). *Mat. Science Forum* **571 – 572**, 189 – 195.

Denks, I. A. (2008). Entwicklung einer Methodik zur Erfassung randschichtnaher Eigenspannungs-verteilungen $\sigma(z)$ in polykristallinen Werkstoffen mittels energydispersiver Diffraktion. Thesis. Universität Kassel (ISBN 978-3-89958-463-9).

Denks, I. A., Manns, T., Genzel, Ch., Scholtes, B. (2009). *Z. Kristallogr. Suppl.* **30**, 69 – 74.

Di Fonzo, S., Jark, W., Lagomarsino, S., Giannini, C., De Caro, L., Cedola, A. & Müller, M. (2000). *Nature* **403**, 638 – 640.

Dölle, H. & Cohen, J. B. (1980). *Metall. Trans. A* **11A**, 159-169.

Eshelby, J. D. (1957). *Proc. Roy. Soc. Lon.* **A241**, 376 – 396.

Genzel, Ch. (2003). In: *Diffraction Analysis of the Microstructure of Materials*, edited by E. J. Mittemeijer & P. Scardi), Springer, Berlin, pp. 473 – 503.

Genzel, Ch., Stock, C., Reimers, W. (2004). *Mat. Sci. Eng. A* **372**, 28 – 43.

Genzel, Ch., Denks, I.A., Gibmeier, J., Klaus, M. & Wagener, G. (2007). *Nucl. Instr. Meth. Phys. Res.* **A578**, 23 – 33.

Genzel, Ch., Denks, I. A., Coelho, R., Thomas, D., Mainz, R., Apel, D. & Klaus, M. (2011a). *J. Strain Analysis* **46**, 615 – 625.

Genzel, Ch., Krahmer, S., Klaus, M. & Denks, I. A. (2011b). *J. Appl. Cryst.* **44**, 1 – 12.Genzel, Ch., Denks, I. A. & Klaus, M. (2012). In: *Modern Diffraction Methods*, edited by E. J. Mittemeijer & U. Welzel, Wiley-VCH, p. 127 – 154.

Greenough, G. B. (1949). *Proc. Royal Soc. (London)* **A197**, 556 – 567.

Hauk, V. & Krug, W. K. (1988), *Härterei-Techn. Mitt.* **43**, 164 – 170.

Hauk, V. (1997). *Structural and Residual Stress Analysis by Nondestructive Methods.* Elsevier, Amsterdam.

Ice, G. E., Budai, J. D. & Pang, J. W. L. (2011). *Science* **334**, 1234 – 1239.

Keckes, J., Bartosik, M., Daniel, R., Mitterer, C., Maier, G., Ecker, W., Vila-Comamala, J., David, C., Schoeder, S. & Burghammer, M. (2012). *Scripta Mat.* **67**, 748 – 751.

Kröner, E. (1958). *Zeitschr. Phys.* **151**, 504-518.

Krywka, C., Neubauer, H., Priebe, M., Salditt, T., Keckes, J., Buffet, A., Roth, S. V., Doehrmann, R. & Müller, M. (2012). *J. Appl. Cryst.* **45**, 85 – 92.

Landolt-Börnstein (1979). *Numerical Data and Functional Relationships in Science and Technology, New Series, Group III, Vol. 11*. Springer, Berlin.

Le Bail, A., Duroy, H., Fourquet, J. L. (1988). *Mat. Res. Bull.* **23**, 447 – 452.

Macherauch, E., Wohlfahrt, H., Wolfstieg, U. (1973). *Härterei Tech. Mitt.* 28, 203 – 211.

Manns, Th. (2010). Analyse oberflächennaher Eigenspannungszustände mittels komplementärer Beugungsverfahren. Thesis. Universität Kassel (ISBN: 978-3-86219-042-3).

Meixner, M., Klaus, M., Genzel, Ch. & Reimers, W. (2013). *J. Appl. Cryst.***46**, 619 –627.

Mittemeijer, E. J. & Welzel, U. (Eds.) (2012). *Modern Diffraction Methods.* Weinheim: Wiley-VCH.

Noyan, I. C. (1983). *Metall. Trans. A* **14A**, 249 – 258.

Noyan, I. C., Cohen, J. B. (1987). In: *Residual Stress, Measurement by Diffraction and Interpretation*, Springer, New York.

Reimers, W., Broda, M., Brusch, G., Dantz, D., Liss, K.-D., Pyzalla, A., Schmackers & T., Tschentscher, T. (1998). *J. Nondestr. Eval.* **17**, 129 – 140.

Reimers, W., Pyzalla, A., Schreyer, A. & Clemens, H. (Eds.) (2008). *Neutrons and Synchrotron Radiation in Engineering. Materials Science: From Fundamentals to Material and Component Characterization*, Wiley-VCH.

Rietveld, H. M. (1967). *Acta Cryst.* **22**, 151 – 152.

Rietveld, H. M. (1969). *J. Appl. Cryst.* **2**, 65 – 71.

Ruppersberg, H., Detemple, I., Krier, J. (1989). *Phys. Stat. Sol.* (a) **116**, 681 – 687.

Ruppersberg, H., Detemple, I., Krier, J. (1995). *Z. Kristallogr.* **195**, 189 – 203.

Ruppersberg, H. (1997). *Mat. Sci. Eng. A* **224**, 61 – 68.

Stefenelli, M., Todt, J., Riedl, A., Ecker, W., Müller, T., Daniel, R., Burghammer, M., Keckes, J. (2013) *J. Appl. Cryst.* **46**, 1378 – 1385.

Thompson, P., Cox, D. E., Hastings, J. B. (1987). *J. Appl. Cryst.* **20**, 79 – 83.

Welzel, U., Ligot, J., Lamparter, P., Vermeulen, A. C. & Mittemeijer, E. J. (2005). *J. Appl. Cryst.*, **38**, 1 – 29.

Withers, P. J. & Webster, P. J. (2001). *Strain* **37**, 19 – 33.

Table 1 Approaches to the description of residual stress depth profiles in real space $\sigma(z)$ and their Laplace transform $\sigma(\tau)$.

$\boldsymbol{\sigma(z)}$	$\boldsymbol{\sigma(\tau)}$	Expression
$\sum_{k=1}^{N} a_k z^k$	$\sum_{k=1}^{N} k!\, a_k \tau^k$	
$a_0 + a_1 e^{-a_2 z}$	$a_0 + \frac{a_1}{a_2\tau + 1}$	P0
$(a_0 + a_1 z) e^{-a_2 z}$	$\frac{a_0}{a_2\tau + 1} + \frac{a_1 \tau}{(a_2\tau + 1)^2}$	P1
$(a_0 + a_1 z + a_2 z^2) e^{-a_3 z}$	$\frac{a_0}{a_3\tau + 1} + \frac{a_1 \tau}{(a_3\tau + 1)^2} + \frac{2a_2\tau^2}{(a_3\tau + 1)^3}$	P2

Table 2 Characteristics of the investigated samples.

Sample	**Geometry**	**Material treatment**
100Cr6	slice (24.4 x 4 mm²)	quenched and tempered (2h at 165°C), surface treatment: grinding + shot peening (Almen intensity: 0.15 – 0.17 mmA, grit: S 110H, coverage: 200%)
α-Al_2O_3	plate (25 x 25 4 mm³)	Surface treatment: grinding + shot peening (grit: HMG, pressure: 2 bar, distance nozzle-sample: 24 mm, peening time: 560 s)

Table 3 Refined values of the parameters of the functions used to describe the in- and out-of-plane stress components $\sigma_{||}(\tau)$ and $\sigma_{33}(\tau)$, respectively, for the shot-peened steel sample. Additionally, the parameters of $\sigma_{||}(\tau)$ without refining $\sigma_{33}(\tau)$ are shown.

Refinement	**a_0**	**a_1**	**a_2**	**a**	**b**
$\sigma_{||}(z)$	-141.65(8.18)	-103.00(1.12)	0.0312($4.1\cdot10^{-4}$)	-	-
$\sigma_{||}(z)$, $\sigma_{33}(z)$	-138.75(8.19)	-104.33(1.14)	0.0317($4.2\cdot10^{-4}$)	$3.787\cdot10^{-5}$ ($8.7\cdot10^{-5}$)	0.01155(0.0114)

Captions

Figure 1 Diagram illustrating the procedure to determine the set of refinable parameters of the model $\sigma_{||}(z)$ (and $\sigma_{||}(\tau)$, respectively) by means of the RIETVELD method. See text for further details.

Figure 2 Shift ΔE of Au diffraction lines with regard to the energy positions calculated from the theoretical lattice parameter a_0^{Au} = 0.4078 nm (zero-crossing) as a function of dead time.

Figure 3 Dead time dependency of the parameters *a*, *b* and *c* of the function (20) used to assign the channel number *ch* to the actual photon energy *E*. The parameters *b* and *c* for the linear and the quadratic term were found to be constant and take values of $8.207 \cdot 10^{-3}$ and $-1.462 \cdot 10^{-9}$, respectively.

Figure 4 Application of the enhanced dead time correction to the calibration measurements shown in Fig. 2. See text for further details.

Figure 5 Real space in-plane residual stress depth distribution in the near surface region of the investigated 100Cr6 sample, shown by the example of the σ_{22} component (Denks, 2008).

Figure 6 Simultaneously RIETVELD refined ED diffraction patterns (selected ψ-positions) of the shot-peened 100Cr6 sample. $\sigma_{||}(z)$ was described using an exponentially damped polynomial of first order (P1 in Tab. 1).

Figure 7 Residual stress depth profiles $\sigma(\tau)^{Rietveld}$ in the LAPLACE space and $\sigma(z)^{Rietveld}$ in the real space obtained by RIETVELD refinement and real space residual stress depth profile $\sigma(z)^{stress-scanning}$ obtained using the stress-scanning method. The parameters a_0, a_1 and a_2 are the refined parameters of the model function used to describe $\sigma(z)^{Rietveld}$. The strain-free lattice parameter used for the refinement was a^{100} = 0.28679 nm. See text for further details.

Figure 8 Comparison of the d_ψ^{exp} vs. $\sin^2\psi$ distributions obtained by conventional whole pattern fitting (see section 2.2 for further details) and the $d_\psi^{hkl}(\tau)$ curves calculated according to $d_\psi^{hkl}(\tau) = \left[\left(\frac{1}{2}S_2^{hkl}\sin^2\psi + 2S_1^{hkl}\right)\sigma_{||}(\tau) + 1\right]d_0^{hkl}$ with $\sigma_{||}(\tau)$ being the LAPLACE transform of the refined residual stress model $\sigma_{||}(z)$. The differences between both curves are shown as a function of energy, ΔE, in order to be used to assess the quality of the refined model for $\sigma_{||}(z)$. Notice that τ depends on $\sin^2\psi$ via equation (12) by substituting $\cos\psi = \sqrt{1-\sin^2\psi}$.

Figure 9 LAPLACE and real space residual stress depth profiles of the 100Cr6 sample obtained for exponentially damped polynomial functions of different order (1st, 2nd and 3rd order or P1, P2 and P3, according to Tab. 1).

Figure 10 Simultaneously RIETVELD refined ED diffraction patterns of the shot-peened Al_2O_3 sample, shown for selected ψ angles. The unfitted smaller peaks at 17.3 keV and 21.1 KeV are escape peaks from the 110 and 113 diffraction lines, respectively.

Figure 11 Residual stress depth profiles $\sigma(\tau)^{Rietveld}$ in the LAPLACE space and $\sigma(z)^{Rietveld}$ in the real space obtained by applying the RIETVELD method. The parameters a_0, a_1 and a_2 are the refined parameters of the model function used to describe $\sigma(z)^{Rietveld}$. The data points shown in the figure were obtained by conventional whole pattern fitting. The refinement was also done using exponentially damped polynomials of higher order (2nd, 3rd, 4th order). The corresponding LAPLACE and real space residual stress depth profiles are shown in the inset.

Figure 12 Comparison of the d_ψ^{exp} vs. $\sin^2\psi$ distributions obtained by conventional whole pattern fitting and the $d_\psi^{hkl}(\tau)$ curves calculated according to the function $d_\psi^{hkl}(\tau) = \left[\left(\frac{1}{2}S_2^{hkl}\sin^2\psi + 2S_1^{hkl}\right)\sigma_{||}(\tau) + 1\right]d_0^{hkl}$.

Figure 13 Triaxial residual stress distribution in the z- as well as in the τ-space as given by the default stress tensor $\sigma(z)$ in equation (23). The strain-free lattice parameter d_0 is assumed to be independent of depth z. Full lines, $\sigma(z)$; dashed lines, $\sigma(\tau)$.

Figure 14 Simultaneously RIETVELD refined ED diffraction patterns from the simulation of the ferrite steel sample, shown for selected ψ angles ($\varphi = 0°$). In total, 64 diffraction patterns were refined simultaneously. Due to the noise added to the simulated patterns and due to the decreasing scale factor with increasing ψ angle the number of diffraction lines that are available for the evaluation reduces with increasing ψ angle.

Figure 15 Triaxial residual stress distributions for intermediate steps and the final refinement obtained by means of the RIETVELD method. (a) All parameters of the 4th order polynomial were refined together but separately for each stress tensor component. (b) The parameters for each stress tensor component were refined together. (c) For σ_{11} four parameters ($a_0^{(11)}$, $a_{0'1}^{(11)}$, $a_2^{(11)}$, $a_4^{(11)}$), for σ_{22} two parameters ($a_0^{(22)}$, $a_4^{(22)}$) and for σ_{33} two parameters ($a_3^{(33)}$, $a_4^{(33)}$) were refined together. (d) Shows the residual stress distribution after the final refinement.

Figure 16 The triaxial residual stress distribution obtained from the RIETVELD refinement compared with the residual stress distribution given by the default stress tensor.

Figure 17 Comparison of the simulated $d_{\varphi\psi}^{110,exp}$ vs. $\sin^2\psi$ distribution (symbols) and the $d_{\varphi\psi}^{110}(\tau)$ curves recalculated using the refined triaxial stress tensor $\sigma(z)$ for the same steps of the refinement as described in the caption of Fig. 15.

Figures

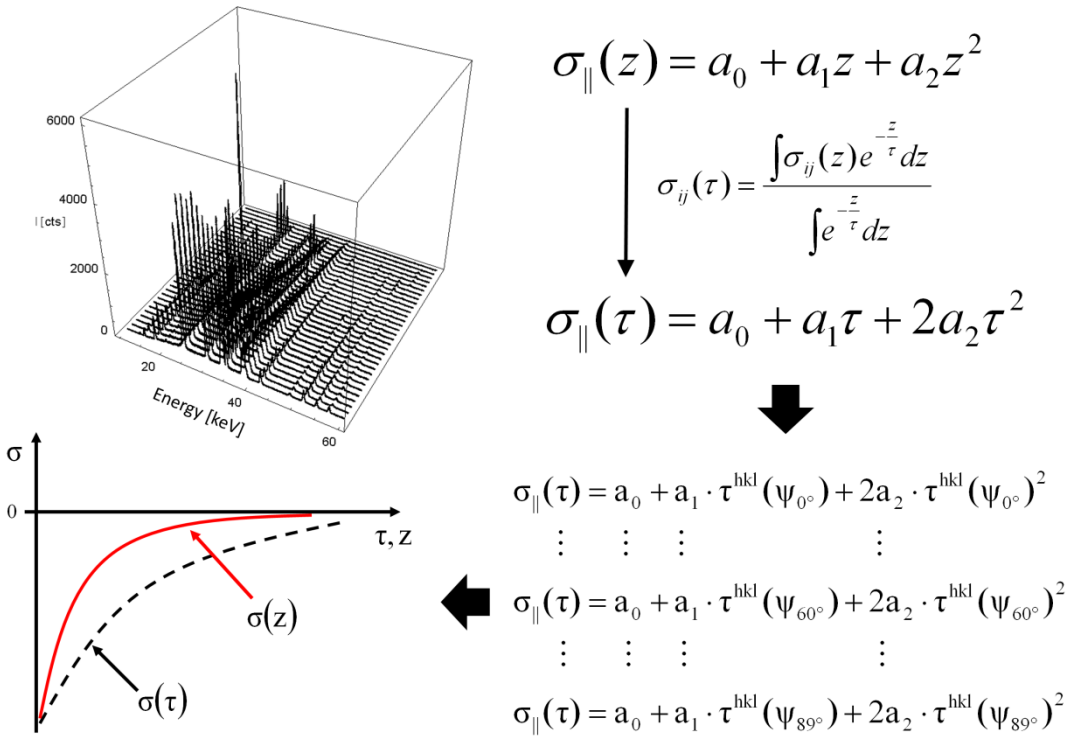

Figure 1

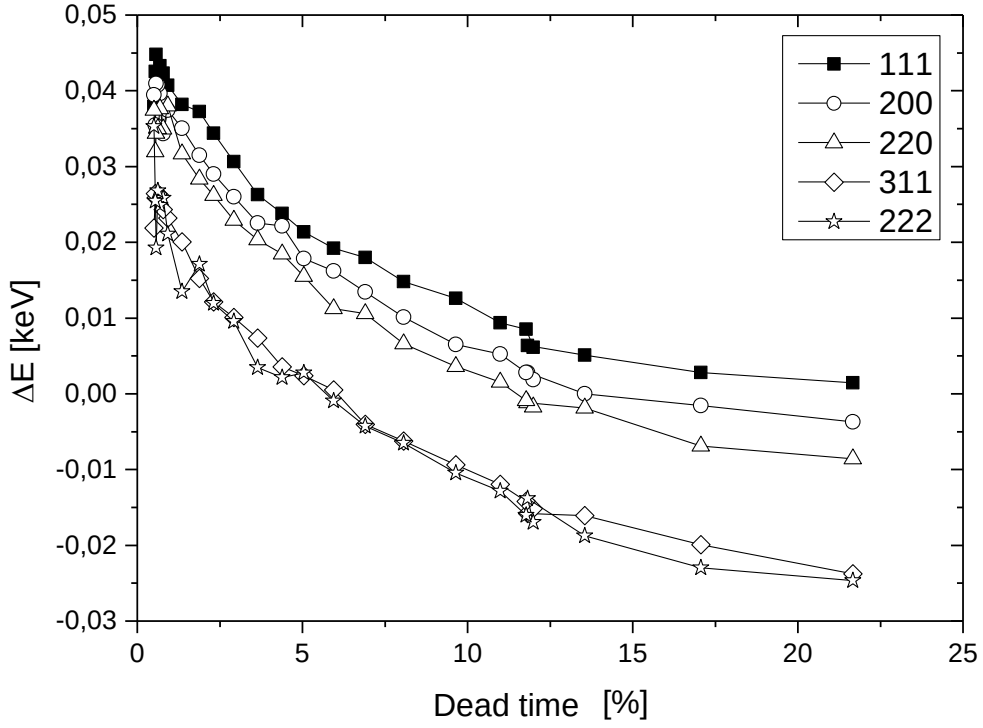
0,05
0,04
0,03
0,02
0,01
0,00
-0,01
-0,02
-0,03
ΔE [keV]
0
5
10
15
20
25
Dead time [%]
111
200
220
311
222

Figure 2

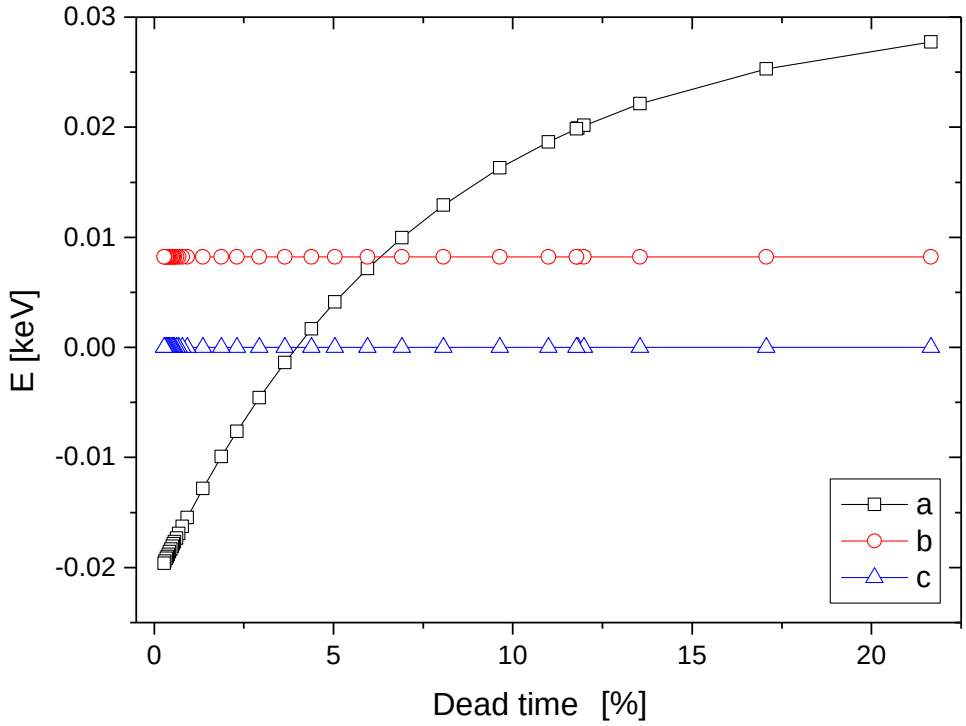

Figure 3

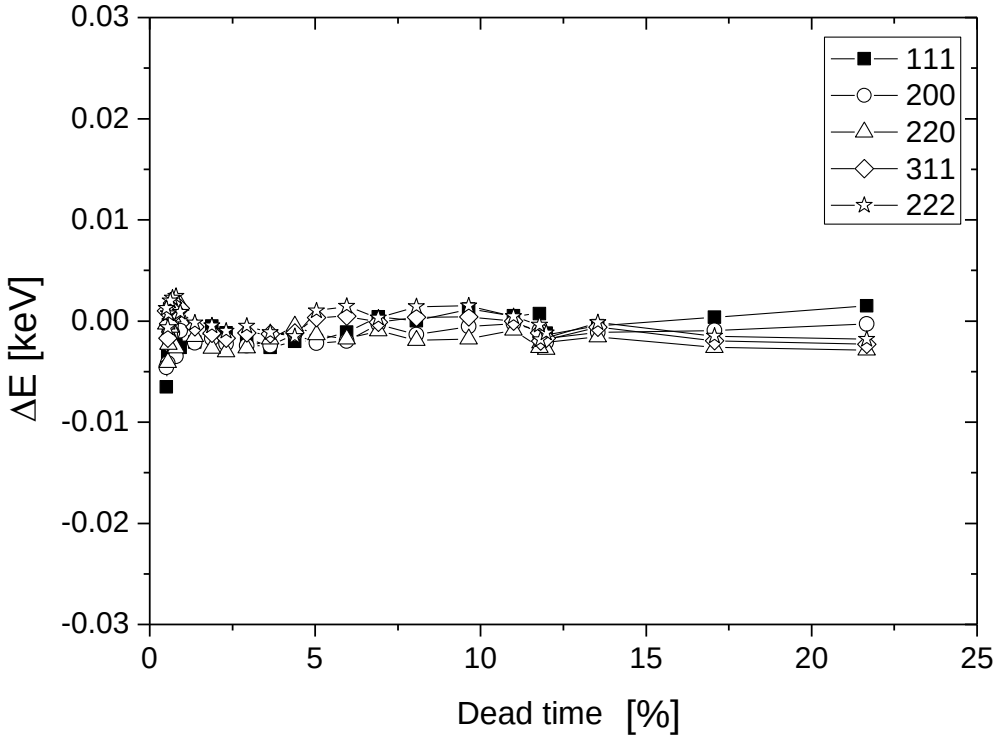
0.03
0.02
0.01
0.00
-0.01
-0.02
-0.03
ΔE [keV]
0
5
10
15
20
25
Dead time [%]
111
200
220
311
222

Figure 4

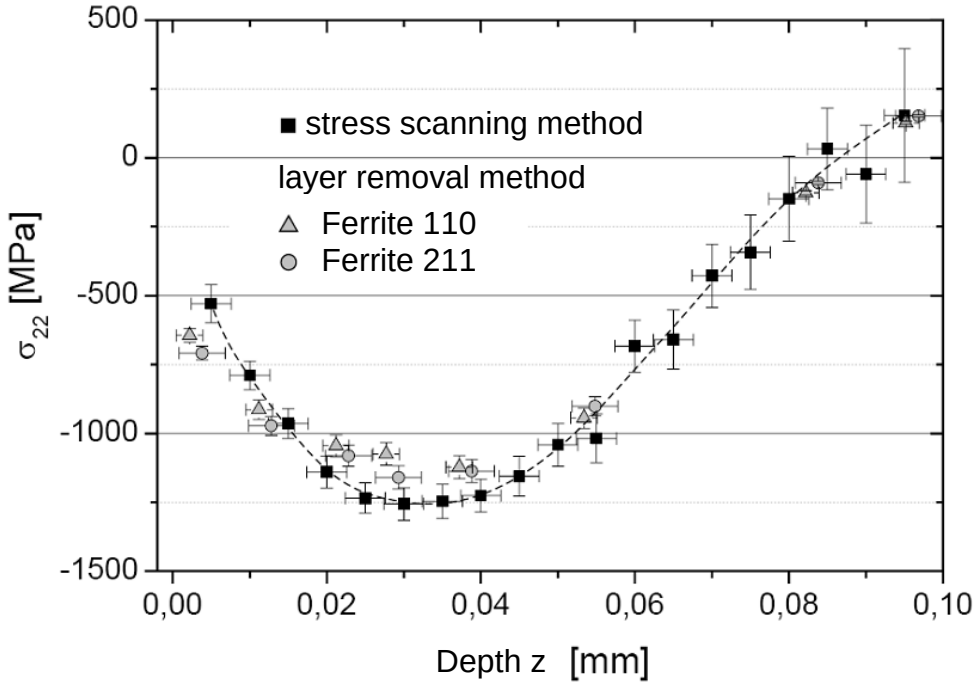
500
0
-500
-1000
-1500
0,00
0,02
0,04
0,06
0,08
0,10
σ22 [MPa]
Depth z [mm]
stress scanning method
layer removal method
Ferrite 110
Ferrite 211

Figure 5

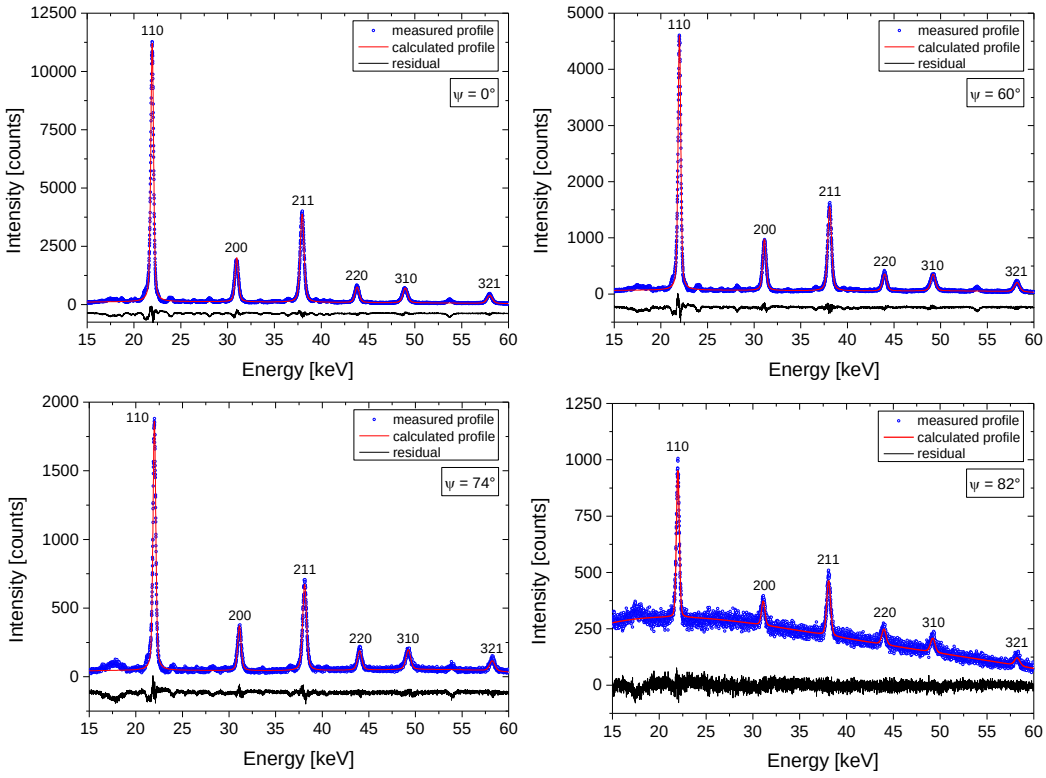
measured profile
calculated profile
residual
ψ = 0°
ψ = 60°
ψ = 74°
ψ = 82°
110
200
211
220
310
321
Intensity [counts]
Energy [keV]

Figure 6

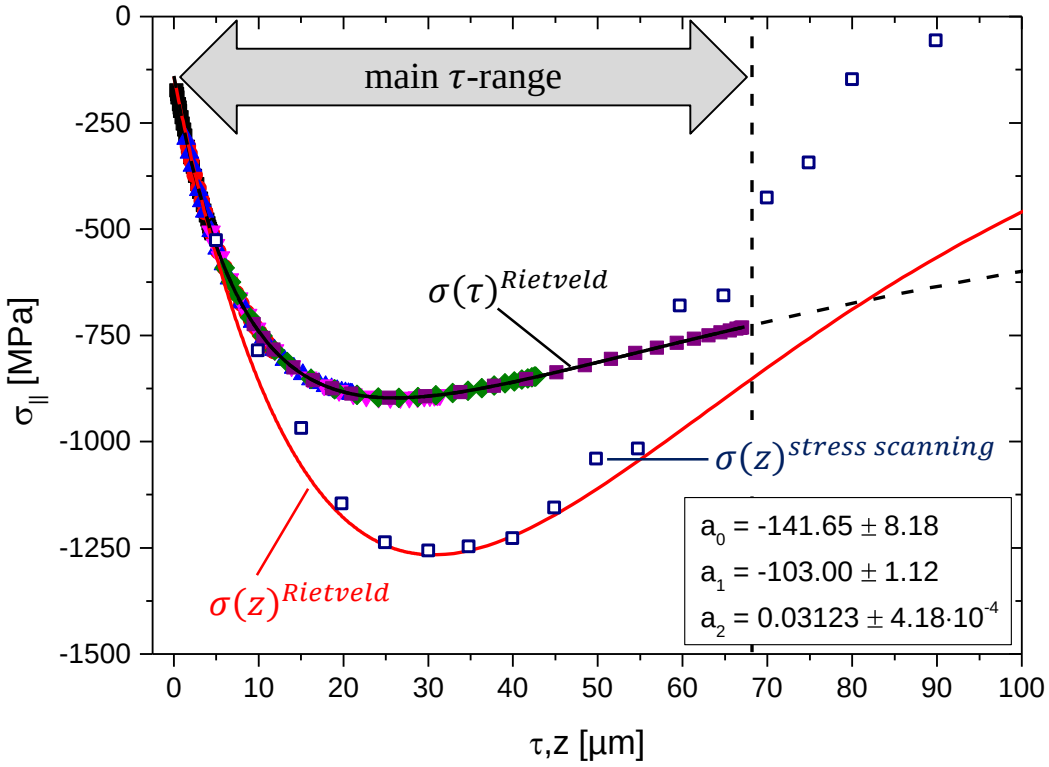
main τ-range
σ(τ)Rietveld
σ(z)stress scanning
σ(z)Rietveld
a0 = -141.65 ± 8.18
a1 = -103.00 ± 1.12
a2 = 0.03123 ± 4.18·10-4
σ|| [MPa]
τ,z [µm]
0
-250
-500
-750
-1000
-1250
-1500
0
10
20
30
40
50
60
70
80
90
100

Figure 7

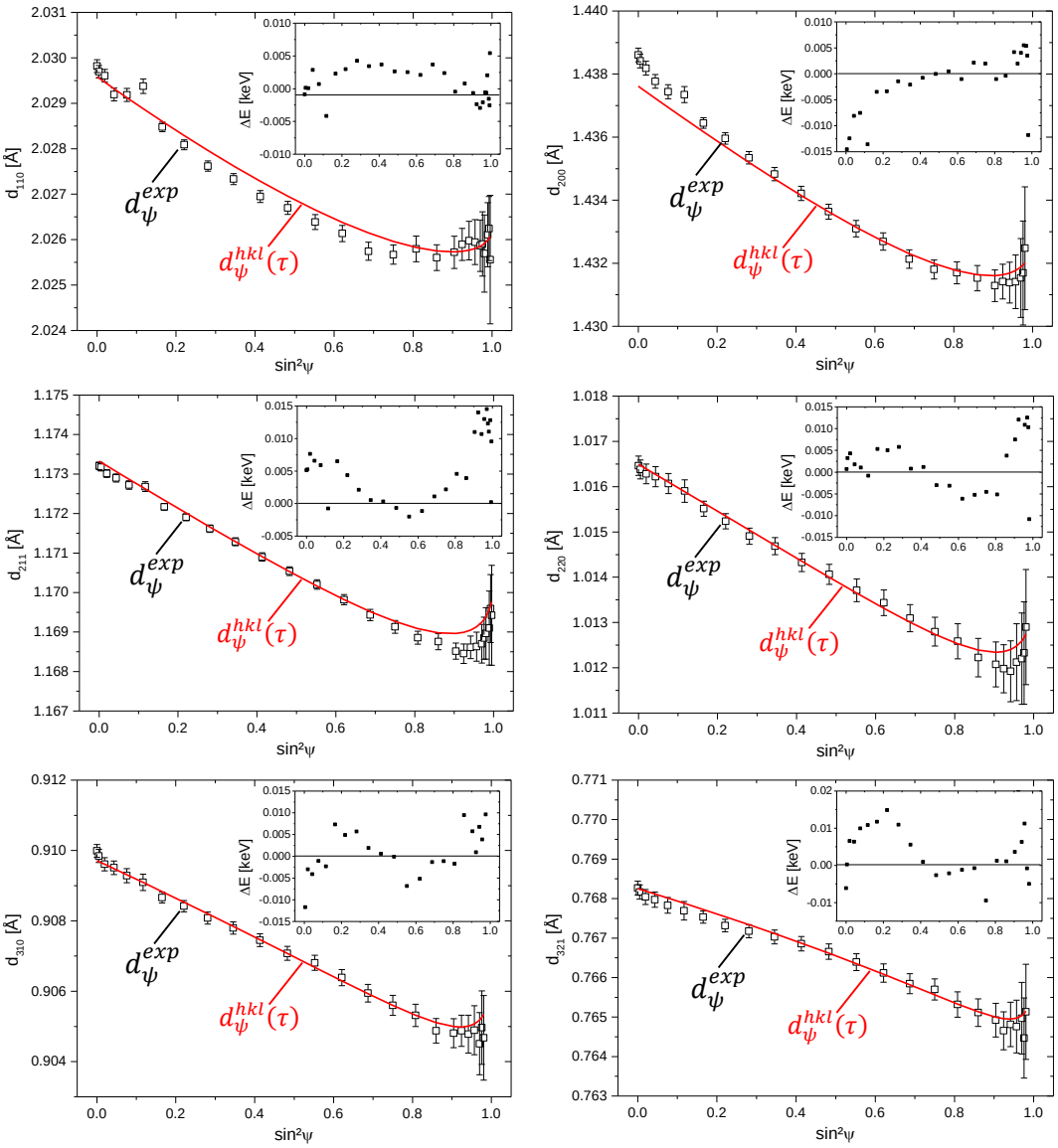
d110 [Å]
d200 [Å]
d211 [Å]
d220 [Å]
d310 [Å]
d321 [Å]
sin²ψ
ΔE [keV]
d_ψ^{exp}
$d_\psi^{hkl}(\tau)$

Figure 8

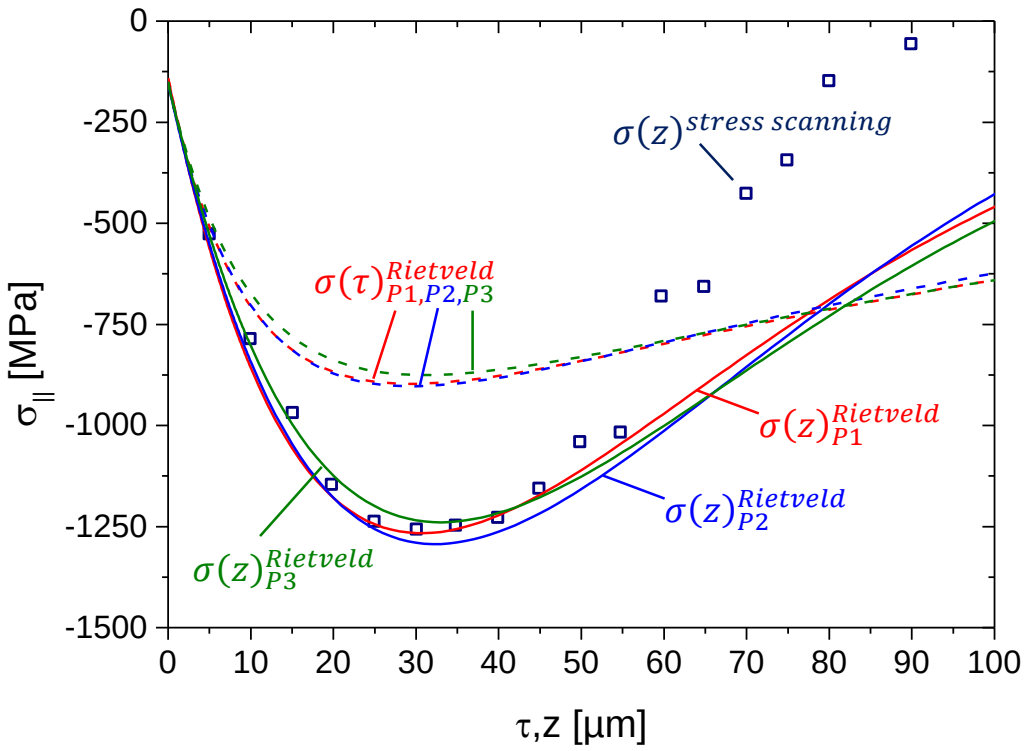
0
-250
-500
-750
-1000
-1250
-1500
σ∥ [MPa]
0
10
20
30
40
50
60
70
80
90
100
τ,z [µm]
$\sigma(z)^{stress\ scanning}$
$\sigma(\tau)^{Rietveld}_{P1,P2,P3}$
$\sigma(z)^{Rietveld}_{P1}$
$\sigma(z)^{Rietveld}_{P2}$
$\sigma(z)^{Rietveld}_{P3}$

Figure 9

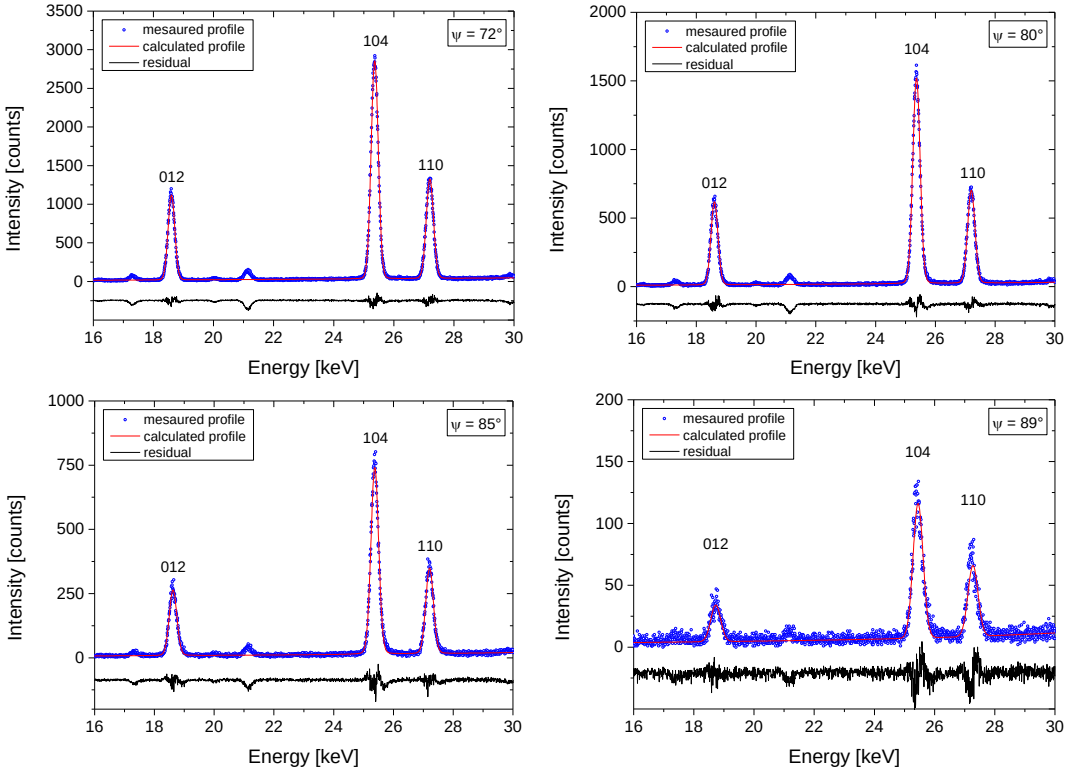
mesaured profile
calculated profile
residual
ψ = 72°
012
104
110
Intensity [counts]
Energy [keV]
ψ = 80°
ψ = 85°
ψ = 89°

Figure 10

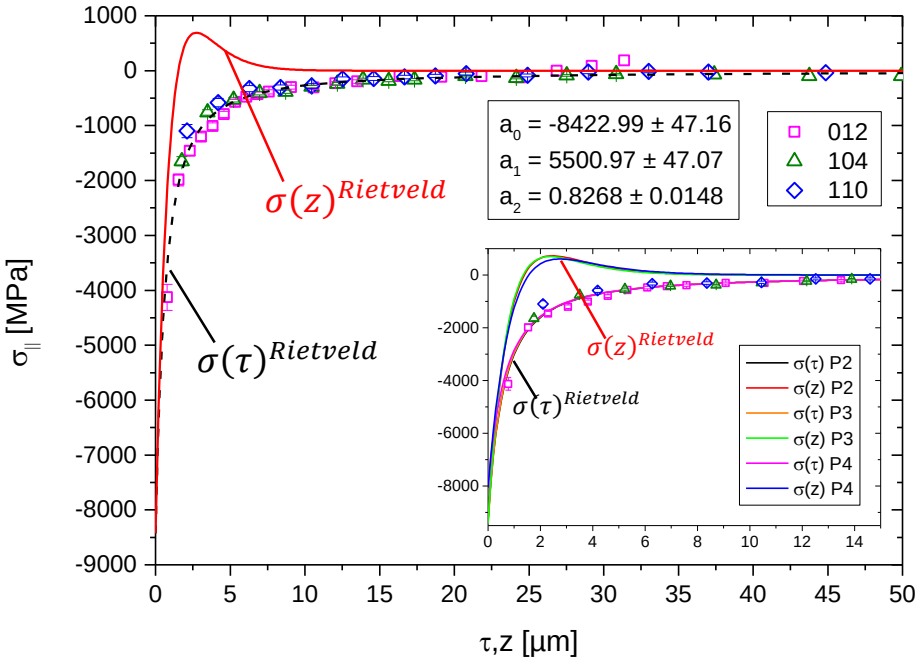
1000
0
-1000
-2000
-3000
-4000
-5000
-6000
-7000
-8000
-9000
σ∥ [MPa]
0
5
10
15
20
25
30
35
40
45
50
τ,z [μm]
a0 = -8422.99 ± 47.16
a1 = 5500.97 ± 47.07
a2 = 0.8268 ± 0.0148
012
104
110
σ(z)Rietveld
σ(τ)Rietveld
σ(τ) P2
σ(z) P2
σ(τ) P3
σ(z) P3
σ(τ) P4
σ(z) P4

Figure 11

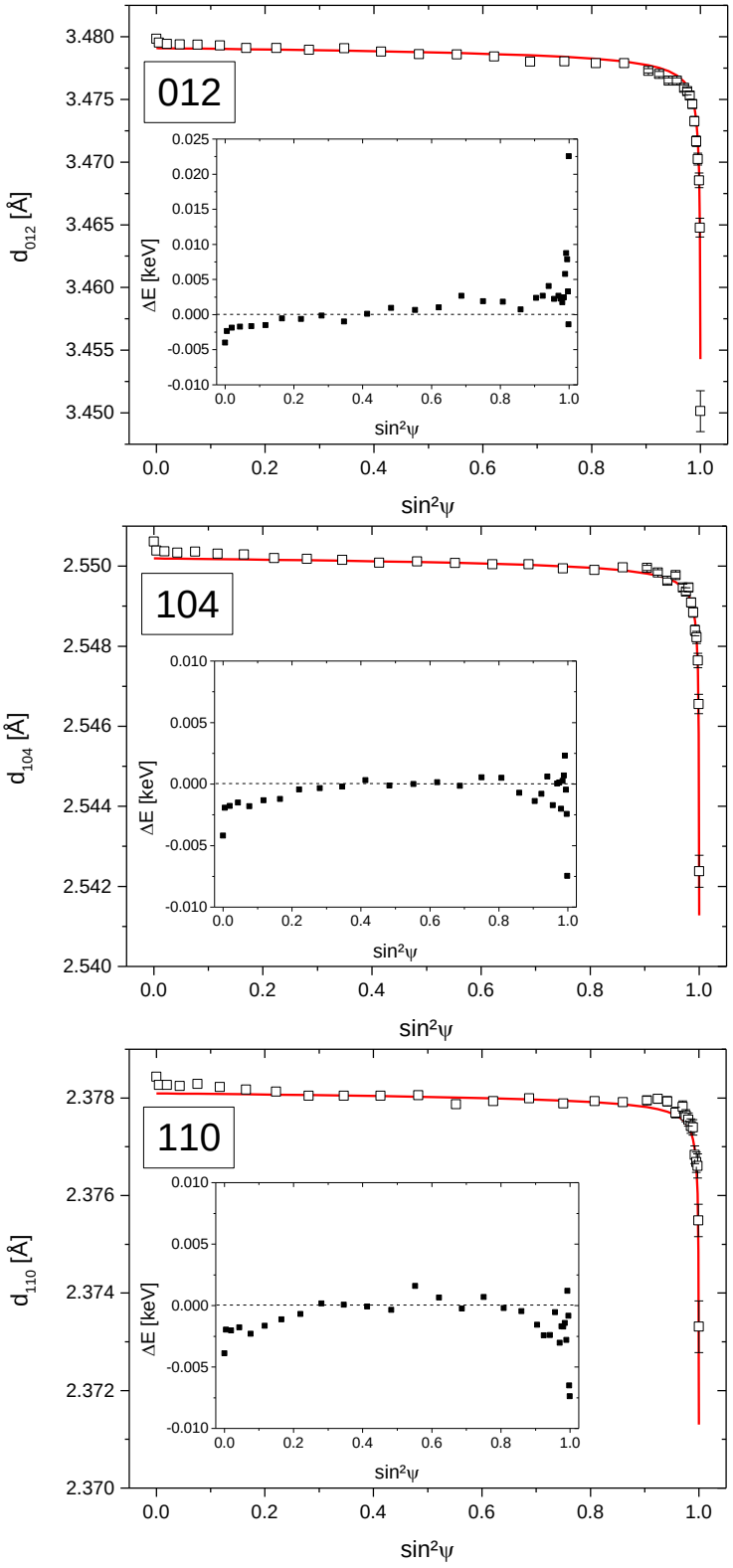

Figure 12

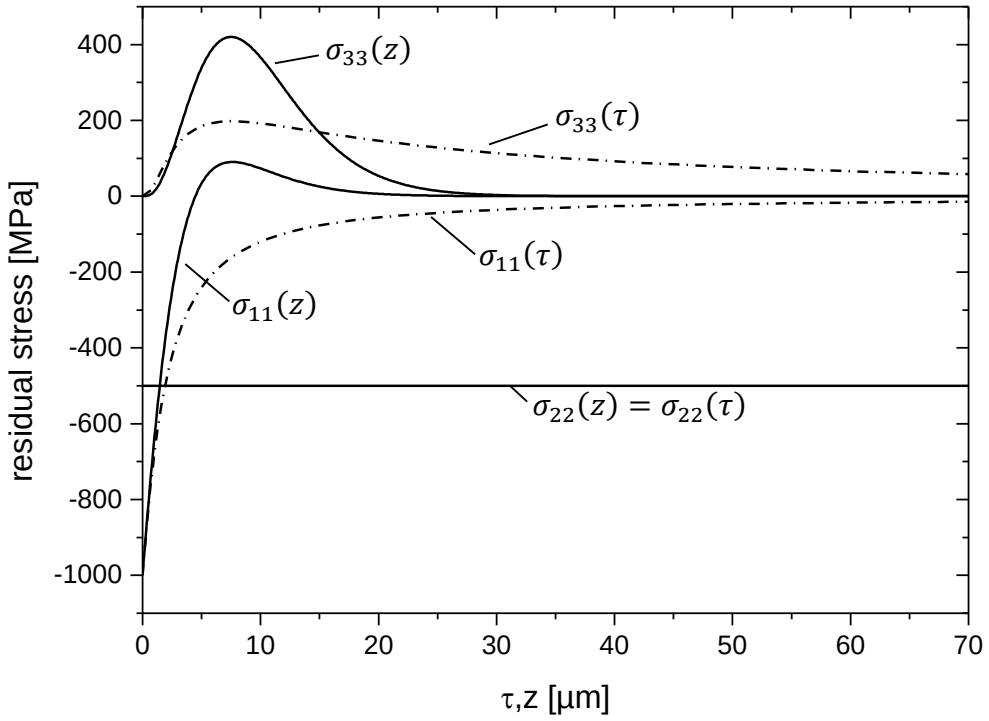
400
200
0
-200
-400
-600
-800
-1000
residual stress [MPa]
0
10
20
30
40
50
60
70
τ,z [μm]
$\sigma_{33}(z)$
$\sigma_{33}(\tau)$
$\sigma_{11}(\tau)$
$\sigma_{11}(z)$
$\sigma_{22}(z) = \sigma_{22}(\tau)$

Figure 13

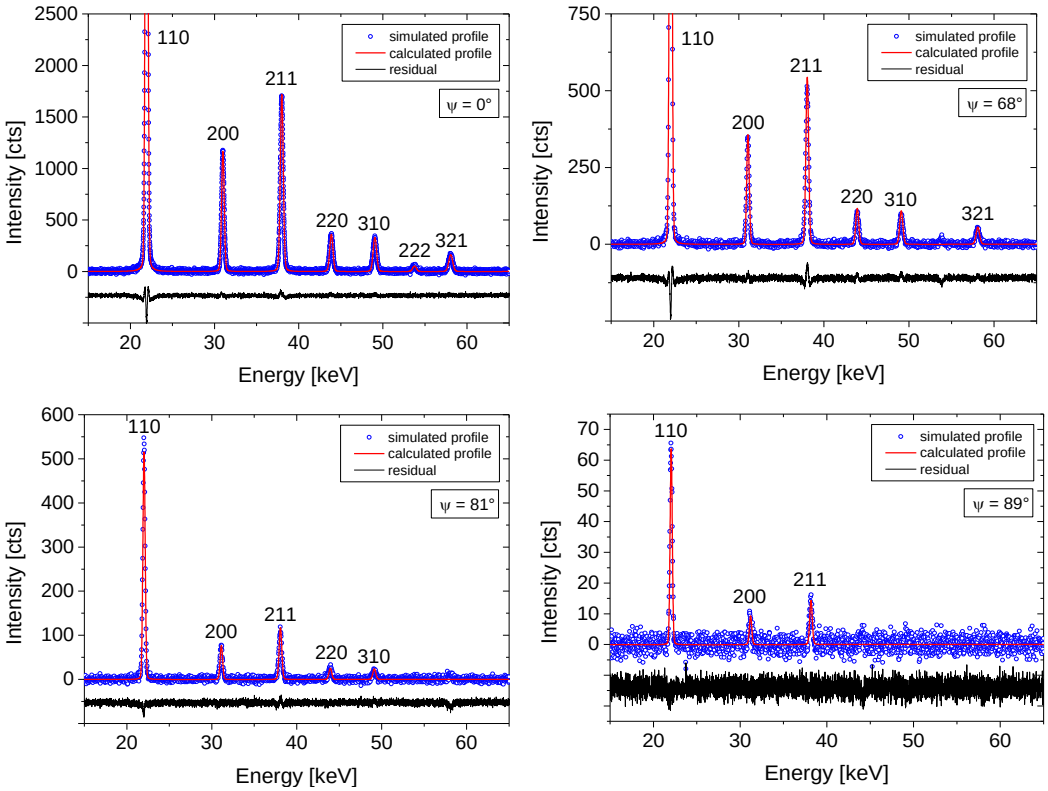
simulated profile
calculated profile
residual
ψ = 0°
ψ = 68°
ψ = 81°
ψ = 89°
110
200
211
220
310
222
321
Intensity [cts]
Energy [keV]

Figure 14

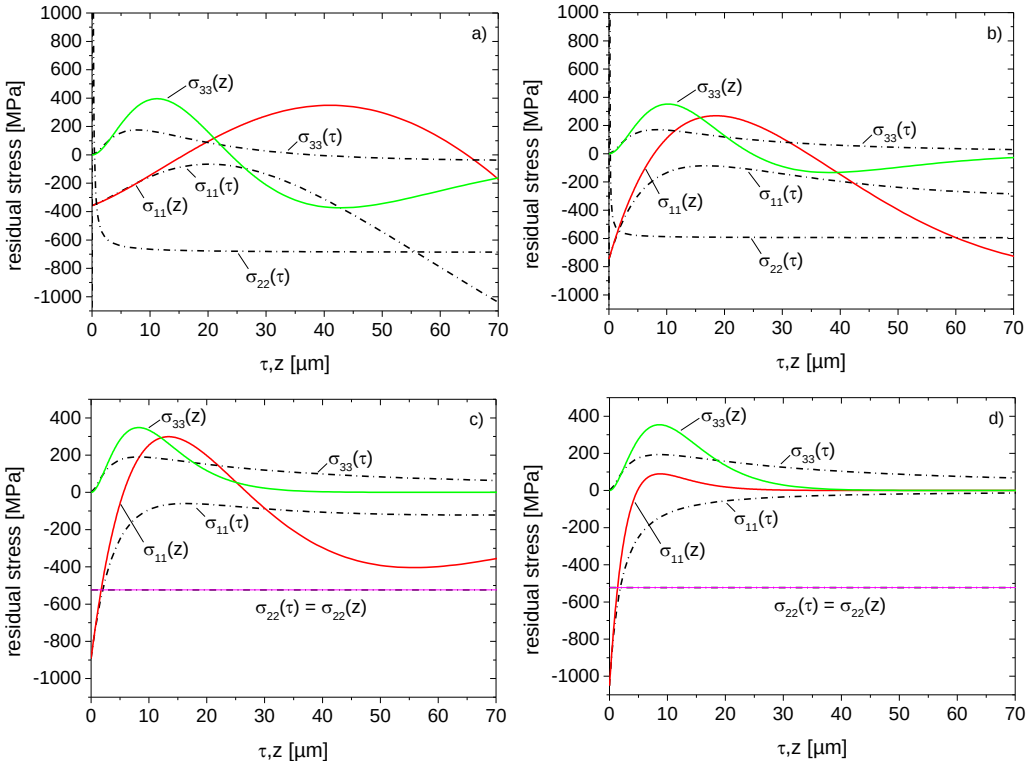
a)
b)
c)
d)
residual stress [MPa]
τ,z [μm]
σ33(z)
σ33(τ)
σ11(z)
σ11(τ)
σ22(τ)
σ22(τ) = σ22(z)

Figure 15

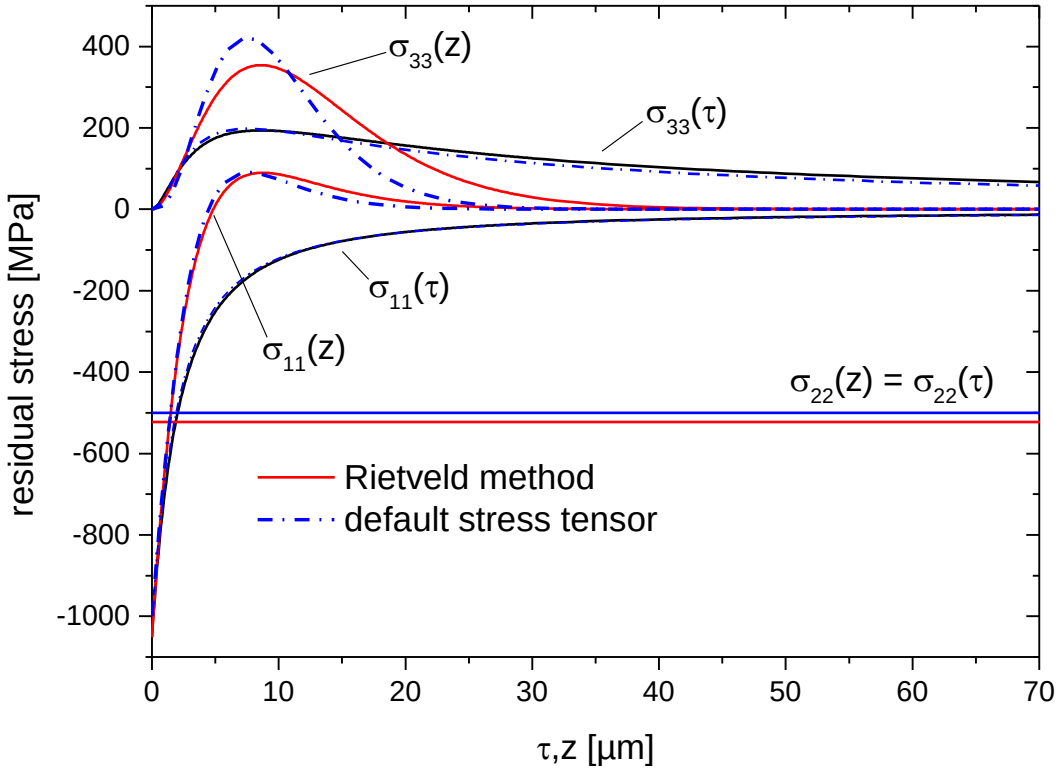
400
200
0
-200
-400
-600
-800
-1000
residual stress [MPa]
0
10
20
30
40
50
60
70
τ,z [μm]
σ33(z)
σ33(τ)
σ11(τ)
σ11(z)
σ22(z) = σ22(τ)
Rietveld method
default stress tensor

Figure 16

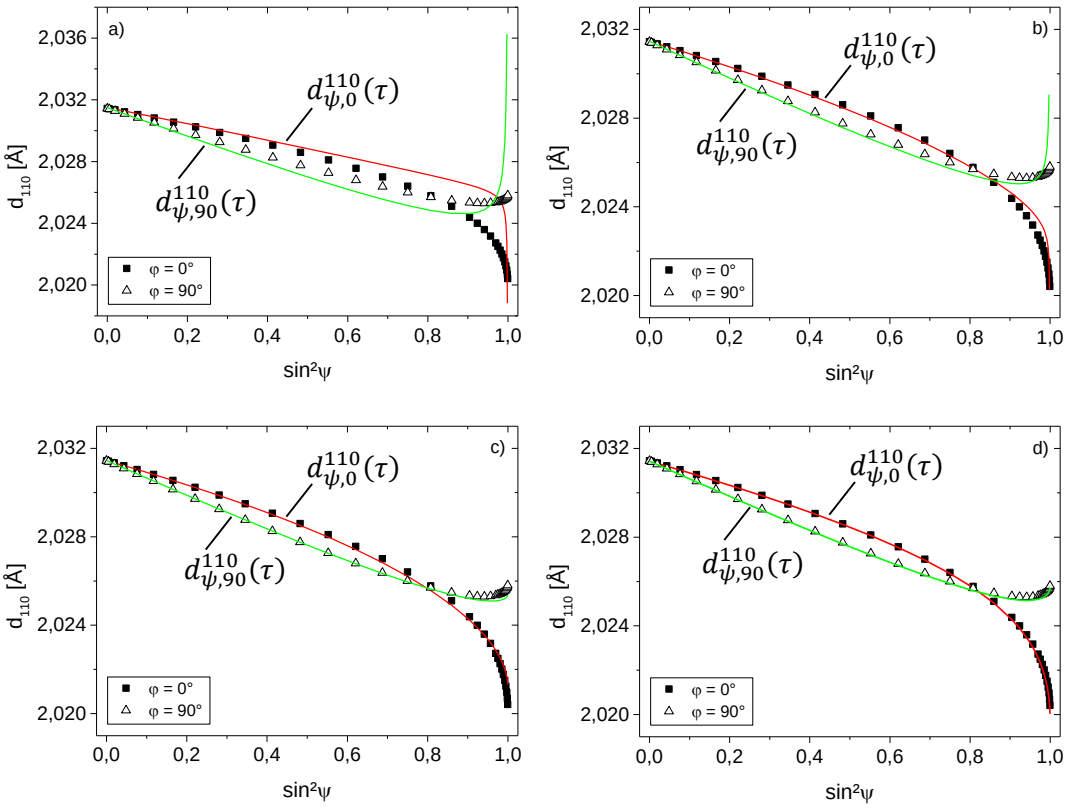
a)
b)
c)
d)
$d^{110}_{\psi,0}(\tau)$
$d^{110}_{\psi,90}(\tau)$
φ = 0°
φ = 90°
d110 [Å]
sin²ψ
2,036
2,032
2,028
2,024
2,020
0,0
0,2
0,4
0,6
0,8
1,0

Figure 17